Modeling of noise-assisted quantum transfer between donor and acceptor with finite bandwidths

Alexander I. Nesterov

Departamento de Física, CUCEI, Universidad de Guadalajara, Av. Revolución 1500, Guadalajara, CP 44420, Jalisco, México and Center for Nonlinear Studies, Los Alamos National Laboratory, Los Alamos, NM 87545, USA

E-mail: `nesterov@cencar.udg.mx`

Gennady P. Berman

Theoretical Division, T-4, Los Alamos National Laboratory and New Mexican Consortium, Los Alamos, NM 87544, USA

E-mail: `gpb@lanl.gov`

Marco Merkli

Department of Mathematics and Statistics, Memorial University of Newfoundland, St. John's, Newfoundland, Canada A1C 5S7 and Center for Nonlinear Studies, Los Alamos National Laboratory, Los Alamos, NM 87545, USA

E-mail: `merkli@mun.ca`

Avadh Saxena

Theoretical Division and Center for Nonlinear Studies, Los Alamos National Laboratory, Los Alamos, NM 87545, USA

E-mail: `avadh@lanl.gov`

Abstract. We present an analytical and numerical study of noise-assisted quantum exciton (electron) transfer (ET) in a dimer consisting of donor and acceptor, modeled by interacting continuous electron bands of finite widths. We start with discrete energy levels for both bands. The interaction with the environment is modeled by a stationary stochastic process (noise) acting on all the donor and acceptor energy levels. Then, by using a continuous limit for the electron spectra, we derive integro-differential equations for the ET dynamics between the two bands. Finally, we derive from these equations rate-type differential equations for the ET dynamics. We formulate the conditions of validity of the rate-type equations. We consider different regions of parameters characterizing the widths of the donor and acceptor bands and the strength of the dimer-noise interaction. For a simplified model with a single energy level donor and a continuous acceptor band, we derive a generalized simple analytic expression and provide numerical simulations for the ET rate. They are consistent with Wigner-Weisskopf, Förster-type, and Marcus-type expressions, in their corresponding regime of parameters. For a weak dimer-noise interaction, our approach leads to the Wigner-Weisskopf ET rate, or to the Förster-type ET rate, depending on other parameters.

In the limit of strong dimer-noise interaction, our approach is non-perturbative in the dimer-noise interaction constant, and it recovers the Marcus-type ET rate. Our analytic results are confirmed by numerical simulations. We demonstrate how our theoretical results are modified when both the donor and the acceptor are described by finite bands. We also show that, for a relatively wide acceptor band, the efficiency of the ET from donor to acceptor can be close to 100% for a broad range of noise amplitudes, for both "downhill" and "uphill" ET, for sharp and flat redox potentials, and for reasonably short times. We discuss possible application of our approach.

1. Introduction

The mathematical modeling of excitonic and electron transfer (ET) in mesoscopic and biological systems has recently attracted much attention [1, 2, 3, 4, 5, 6, 7, 8, 9, 10, 11, 12, 13, 14, 15, 16, 17, 18, 19, 20]. In this respect, the common features of these systems are: (i) the ET takes place between donor and acceptor with finite bandwidths [2, 3, 21, 22, 23] and (ii) the interaction between donor and acceptor bands, and the interaction of the dimer with environment should be taken into account. In real systems, the Hilbert space, which defines the structure of the electron donor (acceptor) energy band (such as the bandwidth and the density of states), can be very complicated [21, 22, 23]. The interaction, $V(E)$, between donor and acceptor bands can be a complicated function of energy, E. The environment, in which the dimer is embedded, is different in different systems. Usually, in theoretical approaches, the environment is modeled by vibrational bosonic modes [6] or by stochastic processes [24, 25, 26, 27, 28]. In particular, the exciton transfer in light harvesting complexes (LHCs) and the electron transfer in primary processes of charge separation in the reaction centers (RCs) of photosynthetic bio-complexes such as plants, eukaryotic algae and cyanobacteria, take place on a very short time-scale, of the order of 0.1 - 10 ps. Generally, these processes (i) involve a heat transfer between the dimer and the environment and (ii) increase the entropy of the dimer (diabatic processes), and they cannot be considered in the framework of the equilibrium statistical approaches. (For discussion see, for example, [7, 8, 9, 10, 11, 12, 13, 29], and references therein.) The mechanisms of interaction between the dimer and the environment are the subjects of many approaches. They include different modifications of the perturbation theory, such as a well-known Redfield theory (RT) [30], modified Redfield theory (MRT) [31], coherent modified Redfield theory (CMRT) [32], polaron transformation [33, 34], non-perturbative approaches [35, 36], hierarchical equations of motion [37, 38], and many others.

One of the main characteristics of the ET processes in these systems is the ET rate. In different regions of parameters, V and λ (interaction with environment), the ET rate has the well-known analytic expressions, such as the Fermi golden rule (perturbation in V and λ) [29]), Förster (modification of Fermi golden rule [29, 39]), Wigner-Weisskopf (wide acceptor band [40, 41]), and Marcus limits (perturbation in V and non-perturbative regime in λ [17, 18, 19]).

The main goal of the present paper is to develop a mathematical approach which gives a simple analytic generalized expression for the ET rate, which has all four limits mentioned above. In order to do this, we consider some simplifications of our model. We study analytically and numerically the ET between the donor and the acceptor, which are modeled by continuous energy bands of finite width, centered at energies, E_0^d and E_0^a, respectively. In order to derive consistently the analytic expression for a generalized ET rate, we start in Sec. 2 with an effective system of corresponding discrete energy levels. The interaction between the donor and acceptor energy levels is

provided by non-diagonal matrix elements, $V_{mn}(E)$, which smoothly depend on energy. The environment is modeled by a stochastic process (telegraph noise) which has two characteristics: the amplitude and the correlation time. Our approach provides: (i) the derivation of a closed set of integro-differential equations for the reduced density matrix (averaged over noise), obtained by taking a continuous limit of a model with discrete electron energy levels, (ii) the derivation of simplified rate-type differential equations describing the ET between interacting donor-acceptor bands with finite bandwidths, and (iii) the identification of the conditions of validity of the rate-type equations.

The distance between the bands, bandwidths, and the intensity of noise can be varied in our theory. This allows us to consider the ET rates and efficiency for narrow or wide electron bands, for bands overlapping to different degrees, and for various noise intensities. Our approach is quite general and can be applied to a variety of systems with noisy environment.

Among our main results are the following.

1) We derive a closed set of the rate-type differential equations for interacting donor-acceptor bands of finite widths and for different intensities of the external noise. These rate-type equations have a simple form, which makes them useful for both theoretical modeling and interpretation of experimental results on ET processes in complex systems.

2) When the donor consists of a single energy level, we obtain an analytic expression for the generalized ET rate. It is consistent with Wigner-Weisskopf, Förster-type, and Marcus-type results in their appropriate regimes. We compare our analytic and numerical results for a continuous acceptor band with the results for the acceptor band consisting of a large number of discrete energy levels.

3) We demonstrate that in the above case 2), there exists an important parameter in the ET rate which includes the electron bandwidths and the dimer-noise interaction constant and which characterizes the asymptotic ET rate for large times.

4) We calculate analytically the ET dynamical rates for two interacting bands. We show the difference in the ET dynamics for two models, when the donor consists of a single level and when it has a band of energies.

5) We find explicitly the conditions of applicability of our approach in all considered limits.

6) We demonstrate that the efficiency of populating the acceptor can be close to 100 % in relatively short times, for both "downhill" and "uphill" redox potentials.

The paper is organized as follows. In Sec. 2, a simplified model is considered in which the donor has a single electron energy level, and the acceptor is modeled by an electron band of finite width. Diagonal noise acts on both the donor and the acceptor. A set of simplified rate-type differential equations is derived. Analytic expressions for time-dependent and asymptotic ET rates are presented. In Sec. 3, we present the results for a generalized model when both, donor and acceptor, are modeled by electron bands of finite width. In Appendix A, we compare the results of a discrete model, when the donor has a single energy level and the acceptor includes many energy levels, with the solutions of the rate-type equations. We also present in Appendix A, the illustration

of application of our results to the dimers based on *Chla* and *Chlb* molecules in LHCs. In the Conclusion, we summarize our results, and discuss possible applications. The Supplemental Material (SM) contains technical details, http://....

2. A simplified model

In this section, we consider a simplified model shown in Fig. 1. A single electron donor site, denoted by the quantum state, $|d\rangle$, interacts with an acceptor site with $2N_a + 1$ ($N_a \gg 1$) quasi-degenerate discrete energy levels.
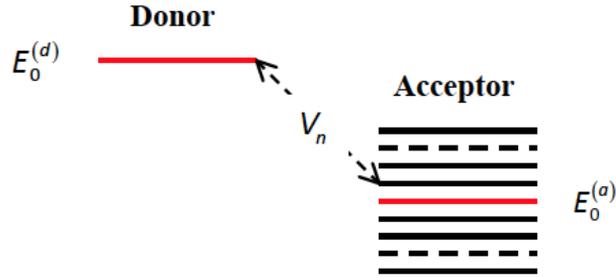
Figure 1. (Color online) Schematic of our simplified model consisting of the donor with a single electron energy level, and the acceptor with a discrete (nearly continuous) electron spectrum. The donor energy level and the center of the acceptor band are indicated by red color.

In the presence of a diagonal noise, the quantum dynamics of the ET can be described by the Hamiltonian [1],

$$\mathcal{H}(t) = (E_0^{(d)} + \lambda_d(t))|d\rangle\langle d| + \sum_{n=-N_a}^{N_a} (E_n + \lambda_a(t))|n\rangle\langle n|$$

$$+ \sum_{n=-N_a}^{N_a} (V_n^*|n\rangle\langle d| + V_n|d\rangle\langle n|), \tag{1}$$

where $E_0^{(d)}$ is the energy level of the donor, $E_0^{(a)}$ is the center of the acceptor band, $\lambda_d(t)$ and $\lambda_a(t)$ describe the noise acting on the donor and the acceptor, respectively. As one can see from (1), this stochastic environment interacts dipole-wise with the dimer. This environment is characterized by two main parameters, the amplitude and the correlation rate (see below), and it describes many non-equilibrium processes, including the spectral density of the protein-solvent fluctuations, polarizability, dimer-environment interaction, and others.

We assume, for simplicity, that the noisy environment, $\xi(t)$, is the same for the donor and the acceptor (collective noise). This assumption is similar to that used in the Marcus theory where thermal protein-solvent environments are considered [17, 18]. One can write $\lambda_d(t) = g_d\xi(t)$ and $\lambda_a(t) = g_a\xi(t)$, where g_d and g_a are the interaction constants. We consider a stationary noise described by a random variable, $\xi(t)$, with

correlation function $\chi(t - t') = \langle \xi(t)\xi(t') \rangle$ and $\langle \xi(t) \rangle = 0$. The averaging, $\langle ... \rangle$, is taken over a random process describing the noise.

We assume that the electron energy spectrum of the acceptor is sufficiently dense, so that E_n and V_n can be considered as continuous variables. Thus, in Eq. (1) one can perform an integration instead of a summation,

$$\mathcal{H}(t) = (E_0^{(d)} + \lambda_d(t))|d\rangle\langle d| + \int (E + \lambda_a(t))|E\rangle\langle E|\varrho(E)dE$$
$$+ \left(\int V(E)|d\rangle\langle E|\varrho(E)dE + \text{h.c.} \right), \tag{2}$$

where, $\varrho(E) = dn(E)/dE$, is the density of electron states of the acceptor, and V_n is replaced by $V(E)$.

We consider a Gaussian density of states (see, for example, [21]) of the acceptor, centered at the energy, $E_0^{(a)}$,

$$\varrho(E) = \varrho_0 e^{-\alpha(E - E_0^{(a)})^2}, \tag{3}$$

where, $\varrho_0 = dn(E)/dE|_{E_0^{(a)}}$, is the density of states at the center of the acceptor band. Formally, the expression (3) allows the existence of energy levels in the acceptor band with very large energies, $|E| \to \infty$, although with very small density of states. To simplify our consideration, we assume that all the $2N_a + 1$ levels of the acceptor band are distributed inside the finite interval, δ_a (acceptor energy band), $[E_0^{(a)} - \delta_a/2, E_0^{(a)} + \delta_a/2]$. Since the number of levels also equals $\int_{-\delta_a/2}^{\delta_a/2} \varrho(E + E_0^{(a)})dE$, we have,

$$2N_a + 1 = \varrho_0 \sqrt{\pi/\alpha}\, \text{erf}(\sqrt{\alpha}\delta_a/2), \tag{4}$$

where, $\text{erf}(z) = (2/\sqrt{\pi}) \int_0^z \exp(-x^2)dx$, is the error function [52]. We define the acceptor bandwidth by $\delta_a = 2\sqrt{\pi/\alpha}$. Employing this expression in Eq. (4), we obtain,

$$\varrho_0 = \frac{4N_a + 2}{\delta_a\, \text{erf}(\sqrt{\pi})}. \tag{5}$$

Using the result (5), Eq. (3) can be written as,

$$\varrho(E) = \frac{4N_a + 2}{\delta_a\, \text{erf}(\sqrt{\pi})} e^{-4\pi(E - E_0^{(a)})^2/\delta_a^2}. \tag{6}$$

Note, that the factor, $\text{erf}(\sqrt{\pi})$, is very close to one: $\text{erf}(\sqrt{\pi}) \approx 0.988$.

The expression (5) allows us to establish a formal relation between the number of levels, $(2N_a + 1)$, in the acceptor of a discrete model (1) and the density of states, ϱ_0, at the center of the acceptor band, in a continuum approach (2). This relation is used below, in numerical simulations, for comparison of these two approaches.

Limit $N_a \to \infty$. It follows from (5), that when the acceptor bandwidth is finite, $\delta_a > 0$, then the density of states satisfies $\varrho_0 \to \infty$ when $N_a \to \infty$, which should be expected. In what follows, we will require that, in this limit, the variance of energy (1) (at $\lambda_{a,d} = 0$) is finite. This requirement involves the initial state of the system. Suppose that initially only the donor is populated. From (1) the variance of energy in the donor

state, $|d\rangle$, is

$$D_d \equiv \langle d|\mathcal{H}^2|d\rangle - \langle d|\mathcal{H}|d\rangle^2 = \sum_{n=-N_a}^{N_a} |V_n|^2 = (2N_a + 1)|V|^2 \equiv v^2 \mathrm{erf}(\sqrt{\pi}),\tag{7}$$

where we have used, for simplicity: $V_n = V$, and $v^2 = V^2 \varrho_0 \sqrt{\pi/\alpha}$ (see below). The requirement $D_d = \mathrm{const}$ means that, when $N_a \to \infty$, the matrix elements, $V_n \to 0$ (or $V \to 0$), and the renormalized matrix element, $v = \mathrm{const}$.

In Fig. 2, the density of states for the acceptor band, centered at $E_0^{(a)} = 0$, is depicted. As one can see, the density of states, $\varrho(E)$, very quickly goes to zero outside of the interval $(-\delta_a/2, \delta_a/2)$. This supports our choice of the relation between α and the acceptor bandwidth: $\delta_a = 2\sqrt{\pi/\alpha}$.
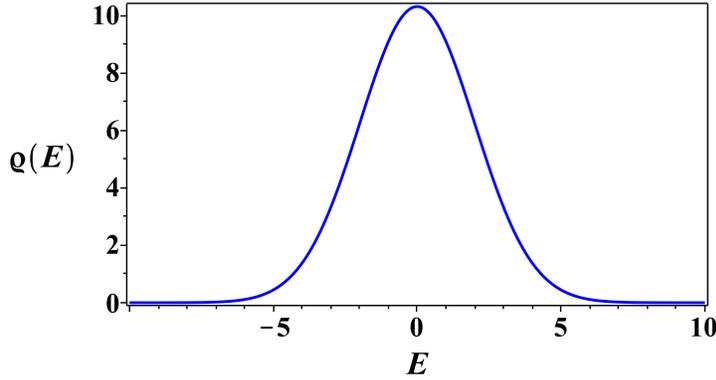
Figure 2. (Color online) Dependence of the density of states, $\varrho(E)$, on the energy, E. Parameters: $N_a = 25$, $\delta_a = 10$.

We denote the donor and acceptor populations (occupation probabilities) at time t, averaged over the noise, by $p_d(t)$ and $p_a(t)$. Suppose that the donor has a single energy level and the acceptor has a continuous energy band. The total donor-acceptor state $\rho(t)$ has matrix elements we denote by $\rho_{dd}(t)$, $\rho_{dE}(t)$, $\rho_{Ed}(t)$ and $\rho_{EE'}(t)$. We have $p_d(t) = \langle \rho_{dd}(t) \rangle$ and $p_a(t) = \int \varrho(E)\langle \rho_{EE}(t)\rangle dE = 1 - p_d(t)$.

We obtain the following system of integro-differential equations for the average of the populations (for technical details, see SM at http://...)

$$\frac{d}{dt}p_d(t) = -\int_0^t K_1(t,t')p_d(t')dt' + \int_0^t K_2(t,t')p_a(t')dt',\tag{8}$$

$$\frac{d}{dt}p_a(t) = \int_0^t K_1(t,t')p_d(t')dt' \quad -\int_0^t K_2(t,t')p_a(t')dt'.\tag{9}$$

The kernels, $K_{1,2}(t,t')$, are found to be,

$$K_1(t,t') = 2v^2 \Phi(t,t')\cos(\varepsilon(t-t'))\exp\left(-\frac{(t-t')^2}{4\alpha}\right),\tag{10}$$

$$K_2(t,t') = 2v^2 \Phi(t,t')\cos(\varepsilon(t-t'))\exp\left(-\frac{t^2+t'^2}{4\alpha}\right),\tag{11}$$

where,

$$\varepsilon = E_0^{(d)} - E_0^{(a)}, \quad v^2 = V^2 \varrho_0 \sqrt{\pi/\alpha}, \tag{12}$$

and $\varphi(t) = (g_d - g_a) \int_0^t \xi(s)ds$, $\Phi(t, t') = \langle e^{i\varphi(t)} e^{-i\varphi(t')} \rangle$ being the characteristic functional of the random process. For the stationary random process $\Phi(t, t') = \Phi(t - t')$.

To arrive at Eqs. 8 - 12, we have modeled the noise by a random telegraph process (RTP) with the correlation function given by [48, 49, 50],

$$\chi(t - t') = \langle \xi(t)\xi(t') \rangle = \sigma^2 e^{-2\gamma(t - t')}, \quad t \geq t'. \tag{13}$$

The RTP includes two parameters, the amplitude of noise, σ, and the decay of correlations, γ. Both these parameters allow one to model the protein-solvent environment in the wide region of functional regimes. In addition, the use of the telegraph noise simplifies significantly the technical part of the mathematical approach, as it allows one to split the high-order correlations into the second order (see SM for detail).

Rate-type equations. One can show (for detail see SM at http:// ...) that if

$$\left| \int_0^t (t - t') K_{1,2}(t, t')dt' \right| \ll 1, \quad t \in (0, \infty), \tag{14}$$

then the integro-differential equations (8) and (9) are well approximated by the rate-type ordinary differential equations

$$\frac{d}{dt}p_d = -\mathfrak{R}_1(t)p_d + \mathfrak{R}_2(t)p_a, \tag{15}$$

$$\frac{d}{dt}p_a = \mathfrak{R}_1(t)p_d - \mathfrak{R}_2(t)p_a, \tag{16}$$

where $\mathfrak{R}_{1,2}(t) = \int_0^t K_{1,2}(t, t')dt'$. We call the functions, $\mathfrak{R}_{1,2}(t)$, the "ET dynamical rates". The rate-type equations (15) and (16) remind us of the Master equations (18) in [53] (see also [54]).

The solution of Eqs. (15) and (16) can be written as,

$$p_d(t) = e^{-f(t)}(1 + \int_0^t \mathfrak{R}_2(s)e^{f(s)}ds), \tag{17}$$

$$p_a(t) = 1 - p_d(t), \tag{18}$$

where, $f(t) = \int_0^t (\mathfrak{R}_1(\tau) + \mathfrak{R}_2(\tau))d\tau$.

On the conditions of applicability of the rate-type equations. The strong conditions of validity of approximation leading to Eqs. (15) and (16) can be written as (see SM at http:// ... for technical details),

$$\frac{|\Delta\rho(t)|}{p_a(t)} \ll 1, \quad \text{and} \quad \frac{v}{p} \ll 1, \tag{19}$$

where $p = \sqrt{\delta_a^2/4\pi + 2(D\sigma)^2}$, and we set $\sigma^2 = \chi(0)$, and $D = g_d - g_a$. The perturbation, $\Delta\rho(t)$, is defined by Eq. (65) in SM.

As one can see, the left inequality in (19) depends on time, and both conditions impose the limitations on the parameters v, ε, and δ_a. The first inequality in Eq. (19)

is related to the derivation of Eqs. (8) and (9). Unfortunately, the explicit analytical form of this condition cannot be obtained, and even its numerical analysis is rather complicated. The condition of applicability, presented by Eq. (14), leads to the second inequality in Eq. (19): $v \ll p$. It allows us to replace the system of integro-differential equations, (8) and (9), by the rate-type equations (15) and (16).

2.1. Estimates of the ET rates

To proceed further, one needs to know the explicit expression for the characteristic functional. We find that $\Phi(t)$ obeys the following integro-differential equation (see SM for detail):

$$\frac{d}{dt}\Phi(t) = -D^2 \int_0^t \chi(t - t')\Phi(t')dt'. \tag{20}$$

When the correlation time of the random process, $\tau_c = (1/\chi(0)) \int_0^\infty \chi(t)dt$, is small enough, $\tau_c \ll 1/|D\sqrt{\chi(0)}|$, one can use the Gaussian approximation and recast (20) as follows:

$$\frac{d}{dt}\Phi(t) \approx -\Phi(t)D^2 \int_0^t \chi(t - t')dt'. \tag{21}$$

The solution of Eq. (21) can be written as

$$\Phi(t) = \exp\left(-D^2 \int_0^t dt' \int_0^{t'} dt'' \chi(t' - t'')\right). \tag{22}$$

When the condition $|d \ln \chi(0/dt)| \ll 3p^2/2\varepsilon$ holds, for computation of the ET rates, $\mathfrak{R}_{1,2}(t) = \int_0^t K_{1,2}(t, t')dt'$, one can use the Gaussian approximation in its simplified form with (see SM for detail)

$$\Phi(t) = \exp\left(-\frac{D^2\chi(0)}{2}t^2\right). \tag{23}$$

For the RTP, with the correlation function (13), we obtain,

$$\Phi(t - t') = \exp\left(-\frac{D^2\sigma^2(t - t')^2}{2}\right). \tag{24}$$

This approximation is valid if the following conditions hold:

$$\tau_c \ll \frac{1}{|D\sigma|} \quad \text{and} \quad \tau_c \gg \frac{2\varepsilon}{3p^2}, \tag{25}$$

where $\tau_c = 1/2\gamma$ is the correlation time of the RTP. The main feature of the Gaussian approximation, in the simplified form (23), is that for the correlation time satisfying the condition $\tau_c \gg 2\varepsilon/3p^2$, the characteristic functional (24) does not depend on γ. Then, this approximation simplifies significantly all the following analytical expressions.

Computation of the ET dynamical rates yields:

$$\mathfrak{R}_1(t) = \frac{\sqrt{\pi}\,v^2}{p} \exp\left(-\frac{\varepsilon^2}{p^2}\right)\left(\text{erf}\left(\frac{pt}{2} + i\frac{\varepsilon}{p}\right) + \text{erf}\left(\frac{pt}{2} - i\frac{\varepsilon}{p}\right)\right), \tag{26}$$

$$\mathfrak{R}_2(t) = \frac{\sqrt{\pi}\,v^2}{p}\left\{\exp\left(-\frac{t^2}{2\alpha} + \frac{(t/2\alpha - i\varepsilon)^2}{p^2}\right)\left(\text{erf}\left(\frac{pt}{2} - \frac{(t/2\alpha - i\varepsilon)}{p}\right)\right.\right.$$
$$\left.\left. + \text{erf}\left(\frac{(t/2\alpha - i\varepsilon)}{p}\right)\right) + \text{c.c.}\right\}. \tag{27}$$

From the properties of the error function it follows that the asymptotic values of rates, $\Gamma_{1,2} = \lim_{t\to\infty} \mathfrak{R}_{1,2}(t)$, are:

$$\Gamma_1 = \frac{2\sqrt{\pi}v^2}{p} e^{-\varepsilon^2/p^2}, \tag{28}$$

$$\Gamma_2 = \begin{cases} \Gamma_1, & \text{if} \quad \delta_a = 0, \\ 0, & \text{if} \quad \delta_a \neq 0, \end{cases} \tag{29}$$

where $0 \leq p < \infty$. Note, that, at a given value of ε, $\Gamma_1(p = 0) = 0$ and $\Gamma_1(p \to \infty) \to 0$. The maximum of the asymptotic ET rate (28) corresponds to the "resonant" condition,

$$p_{res} = \sqrt{2}\varepsilon, \tag{30}$$

and the maximum of the ET rate (28) is,

$$\Gamma_1^{(max)} = \sqrt{\frac{2\pi}{e}} \frac{v^2}{\varepsilon}. \tag{31}$$

The ET rate (28) approaches zero at parameter $p = 0$ and at $p = \infty$. It has a maximum at p_{res} (30). The physical reason for this is rather simple: When $p = 0$, there is no external random force. When $p = \infty$, the external random force is so large, that the system cannot follow the excitation. In the Marcus theory (thermal environment) the ET rate also experiences maximum (resonance) at some value of the interaction constant between the dimer and the environment.

We find that the leading terms in Eqs. (26) and (27), as $t \to \infty$, are:

$$\mathfrak{R}_1(t) = \Gamma_1 \left(1 + \mathcal{O}\left(\frac{e^{-pt}}{\sqrt{\pi}\,pt} \right) \right), \tag{32}$$

$$\mathfrak{R}_2(t) \sim \Gamma_1 \cos\left(\frac{\varepsilon t}{\alpha p^2} \right) \exp\left(-\nu t^2 \right), \tag{33}$$

where,

$$\nu = \frac{2p^2 - 1/\alpha}{4\alpha p^2}. \tag{34}$$

Note on the asymptotic limits. The expression (28) for Γ_1 can be considered as a generalized ET rate for a single-level ("zero bandwidth") donor and a finite bandwidth acceptor. As we show below, it reduces to (i) the Wigner-Weisskopf ET rate for an infinitely wide acceptor band, and for any intensity of dimer-noise interaction constant, (ii) the modified Wigner-Weisskopf (or Förster-type) ET rate for weak dimer-noise interaction and finite bandwidth, and (iii) the Marcus-type ET rate, for relatively strong dimer-noise interaction, when the regular perturbation approach for dimer-environment interaction cannot be used.

It is important to note, that in the case of a single-level donor and a finite band acceptor, the ET rate, (28), is finite even at $t \to \infty$. This results in re-population of the donor-acceptor complex during the time-interval $0 \leq t < \infty$. As we show below, this situation changes for a finite bandwidth donor. On the other hand, for any finite bandwidth, $\delta_a \neq 0$, of the acceptor, the asymptotic rate satisfies $\Gamma_2 = 0$. This rate provides a re-population of the ET dynamics only during finite times.

Our analytical results, (28) and (29), are confirmed by the results of our numerical simulations for a continuous model, (15) and (16), presented in Figs. 3 - 6, for different values of parameters characterizing the bandwidth and the intensity of noise.

In the numerical simulations, we measure all energy parameters in units of ps^{-1}, and time is measured in ps. The values of parameters in the energy units can be obtained by multiplying our values by $\hbar \approx 6.58 \times 10^{-13} \mathrm{meV}$. For example, $\varepsilon = 60\,\mathrm{ps}^{-1} \approx 40\,\mathrm{meV}$.

2.2. Dependence of asymptotic ET rate on acceptor bandwidth and strength of dimer-noise interaction

We use the expression (28) to describe the ET rates of the system. In the rest of the paper, it is assumed that initially only the donor is populated. We will analyze two limits: the "narrow" acceptor band, when $\delta_a \ll \varepsilon$ (the donor and the acceptor band do not overlap) and the "wide" acceptor band, when $\delta_a \gg \varepsilon$ (the donor overlaps with the acceptor band). We also define the "weak dimer-noise interaction" regime by $|D\sigma| \ll \delta_a/\sqrt{8\pi}$, and the "strong dimer-noise interaction" regime to be the opposite limit, when $|D\sigma| \gg \delta_a/\sqrt{8\pi}$.

2.2.1. Weak dimer-noise interaction
For weak dimer-noise interaction, one can neglect the contribution of $D\sigma$, and write $p \approx \delta_a/2\sqrt{\pi}$. Substituting p into Eq. (28), we obtain,

$$\Gamma_1 = \frac{4\pi v^2}{\delta_a}\, e^{-4\pi\varepsilon^2/\delta_a^2}. \tag{35}$$

Förster-type ET rate. If we take into account the relation, $v^2 = V^2 \varrho_0 \sqrt{\pi/\alpha}$, then expression (35) becomes

$$\Gamma_1 = 2\pi V^2 \varrho_0 e^{-4\pi\varepsilon^2/\delta_a^2}. \tag{36}$$

The ET rate (36) can be interpreted as the Wigner-Weisskopf-type ET rate with the renormalized electron density of states, $\varrho_0 \to \varrho_0 \exp(-4\pi\varepsilon^2/\delta_a^2)$. We will call it the Förster-type ET rate. It differs from the Wigner-Weisskopf-type ET rate by the factor, $\exp(-4\pi\varepsilon^2/\delta_a^2)$, which characterizes the overlap between the donor energy level and the acceptor band.

In Fig. (3), we illustrate the Förster-type ET dynamics for weak dimer-noise interaction and for a partial overlapping of the donor level with the acceptor band ($\varepsilon \ll \delta_a$). One can see a good agreement between the solutions of Eqs. (15) and (16) (green and blue solid curves) with the plots presented by dashed and dash-dotted curves corresponding to the rate given by Eq. (36).

Wigner-Weisskopf-type ET rate. For $\varepsilon \ll \delta_a/2\sqrt{\pi}$ (very wide band), the ET rate can be written as,

$$\Gamma_1 = 2\pi V^2 \varrho_0 = 4\pi v^2/\delta_a, \tag{37}$$

which coincides with the Wigner-Weisskopf-type ET rate [40, 41].
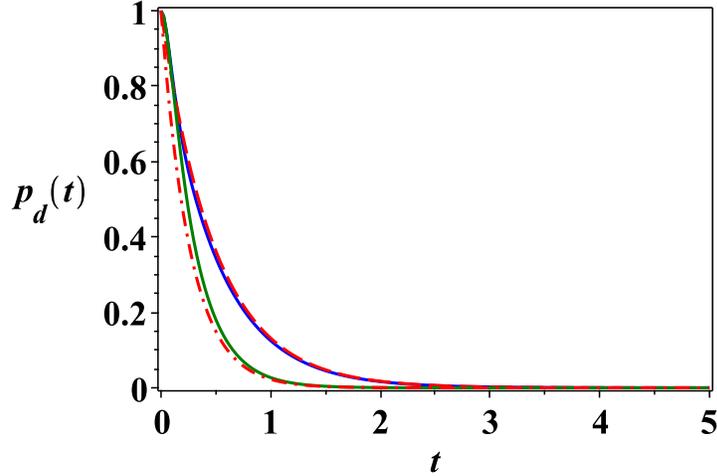
Figure 3. (Color online) Dependence of $p_d(t)$ on time, for the Förster-type ET rate: solutions of Eqs. (15) and (16) (green and blue solid curves). Parameters: $v = 5$, $D\sigma = 0.01$, $\delta_a = 50$; $\varepsilon = 10$ (green and red dash-dotted curves); $\varepsilon = 15$ (blue and red dashed curves). Plots presented by dashed and dash-dotted curves correspond to the rate given by Eq. (36).

Relation to Heisenberg uncertainty principle. Note, that the rate (37) has a simple connection with the Heisenberg uncertainty relation. Indeed, Γ_1 (37) can be written as:

$$\Gamma_1 = 4\pi(v/\delta_a)v < v, \tag{38}$$

where we have used the inequality, $v \ll \delta_a$, which means that $\sqrt{D_d}$ in (7), is significantly smaller than the acceptor bandwidth. If we use for tunneling time in (37), $\Delta t_d \sim 1/\Gamma_1$, and for energy uncertainty from (7), $\Delta E_d = \sqrt{D_d} \sim v$, we have from (38) the Heisenberg uncertainty relation: $\Delta E_d \Delta t_d > 1$.

Fermi's golden rule. The expression (37) means that the probability of population of the acceptor band is $p_a(t) = 1 - \exp(-\Gamma_1 t)$. For $\Gamma_1 t \ll 1$, we get $p_a(t) \approx \Gamma_1 t$, which corresponds to the Fermi's golden rule [29].

The dynamics of the donor population is illustrated, for weak dimer-noise interaction and wide band (the Wigner-Weisskopf limit), in Fig. 4. The following parameters were chosen: $v = 1$, $\varepsilon = 0$, $D\sigma = 0.01$ and $\delta_a = 20$. In this case, noise does not make a contribution to the ET rate, and the population of the acceptor is determined by the "entropy factor" – the continuous electron energy spectrum of the acceptor band. The case of weak dimer-noise interaction and narrow band, which is close to a two-level system, is discussed in Appendix A.

2.2.2. Strong dimer-noise interaction In this case we have $p \approx \sqrt{2}D\sigma$ and for both, narrow and wide bands, (28) gives the Marcus-type expression for the ET rate,

$$\Gamma_1 = v^2 \sqrt{\frac{2\pi}{D^2\sigma^2}} \exp\left(-\frac{\varepsilon^2}{2D^2\sigma^2}\right). \tag{39}$$
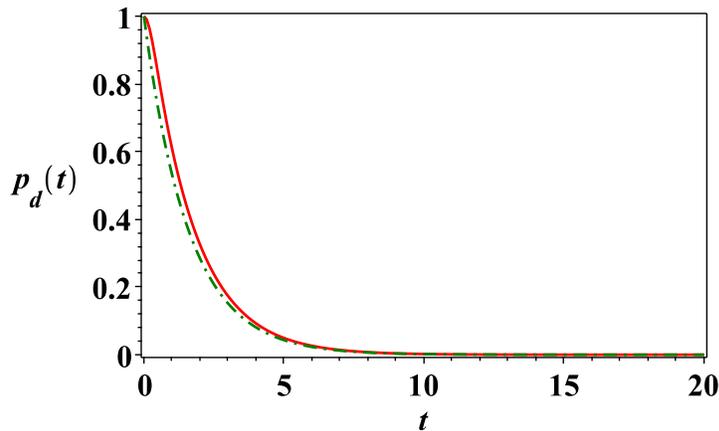
Figure 4. (Color online) Dependence of $p_d(t)$ on time, for the Wigner-Weisskopf-type ET rate: solution of Eqs. (15) and (16) (red curve); green dash-dotted curve corresponds to the asymptotic rate (37). Parameters: $v = 1$, $\varepsilon = 0$, $D\sigma = 0.01$, $\delta_a = 20$.

This result is similar to the Marcus ET rate for a donor-acceptor complex, modeled by a two-level system, having strong interaction with the environment, [18, 19], even though for the latter one considers a thermal noise.

As one can see from (39), the dimer-noise interaction, $D\sigma$, represents, in the Marcus-type limit, a "singular perturbation", and the ET rate (39) cannot be derived by using a regular perturbation theory in $D\sigma$.

Our analytic prediction (39) is confirmed by the numerical simulations of Eqs. (15) and (16), presented in Fig. 5 (for strong dimer-noise interaction and relatively narrow band) and in Fig. 6 (for strong dimer-noise interaction and wide band). In Fig. 5, $p_d(t)$ is shown for different values of the dimer-noise interaction constant, $D\sigma$, and for a relatively narrow band, δ_a. In Fig. 6, the donor population is given for a relatively wide acceptor band.

2.2.3. **Notes on reorganization energy.** In our approach, we model the protein-solvent environment by a stochastic process (stationary telegraph noise), which has two main characteristics: the amplitude and the correlation rate. This approach is similar to those used in [24, 25, 26, 27, 28]. Many approaches in bio-systems are based on the thermal environment, which is described by non-commuting quantum bosonic operators (such as in [18, 19]). Note, that it would be very desirable to verify experimentally the conditions of applicability of both noisy and thermal environments for very fast ET processes in bio-complexes, when the thermal relaxation times significantly exceed the times of ET processes.

As it should be expected, the symmetric stochastic process, with $\bar{\xi}(t) = 0$, leads to a vanishing reorganization energy in the Marcus-type expression for the ET rate (39). As shown in [51] (see Eq. (40)), one way to introduce a reorganization energy in our
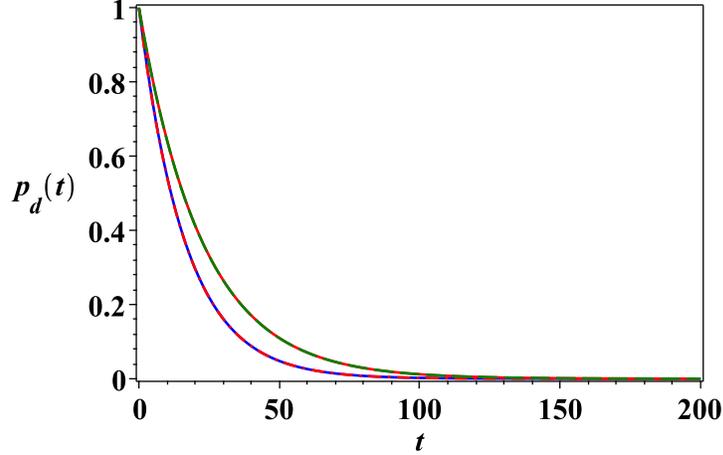
Figure 5. (Color online) Marcus-type ET rate. Strong dimer-noise interaction and narrow band. Dependence of $p_d(t)$ on time, t ($v = 1$, $\varepsilon = 25$, $\delta_a = 5$). From the top to bottom, $D\sigma = 50$ and $D\sigma = 25$. Solid curves correspond to the solutions of Eqs. (15) and (16). Dashed curves correspond to the rate given by Eq. (39).
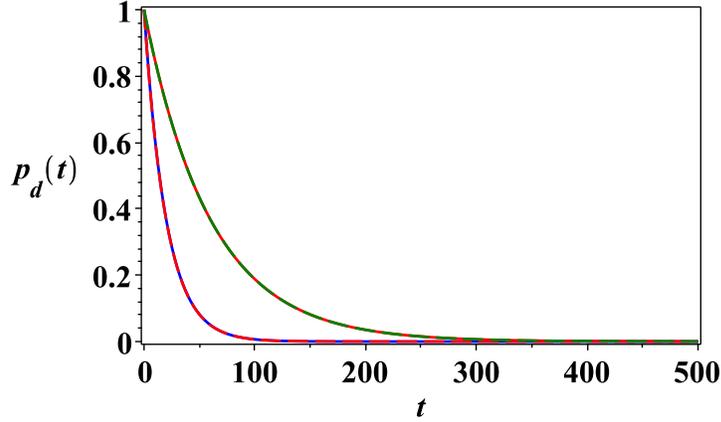
Figure 6. (Color online) Marcus-type ET rate. Strong dimer-noise interaction and relatively wide band. Dependence of $p_d(t)$ on time, t ($v = 1$, $\varepsilon = 1$, $\delta_a = 10$). From the top to bottom, $D\sigma = 150$ and $D\sigma = 50$. Solid curves correspond to solutions of Eqs. (15) and (16). Dashed curves correspond to the rate given by Eq. (39).

approach is to use 'a "non-symmetric" stochastic process with $\langle \xi(t) \rangle \equiv \bar{\xi} \neq 0$. In this case, the renormalized redox potential becomes, $\varepsilon \to \varepsilon - \lambda$, where $\lambda = D\bar{\xi}$ is the effective "reorganization energy". Then, the ET rate in (39) can be rewritten as [51],

$$\Gamma = v^2 \sqrt{\frac{2\pi}{D^2\sigma^2}} \exp\left(-\frac{(\varepsilon - \lambda)^2}{2D^2\sigma^2}\right). \tag{40}$$

At the same time, the "reorganization energy" in (40) differs from the reorganization energy, ε_{rec}, in Marcus theory, where $\varepsilon_{rec} \propto \lambda^2$, and has a different meaning and dependence on parameters of the thermal environment [18, 19]. We call ET rate (40) the

Marcus-type rate because, similar to the Marcus theory, this rate (i) is a perturbative result in the donor-acceptor interaction, v, (ii) is a non-perturbative result in the dimer-environment interaction, $D\sigma$, (has the interaction constant, $D\sigma$, in the denominator) and (iii) has a similar form as the Marcus ET rate.

2.3. Uphill ET $(\varepsilon < 0)$

Until now, we have discussed the "downhill ET" $(\varepsilon > 0)$ in the donor-acceptor photosynthetic complex. This situation in rather common–the energy of the donor band is positioned above the energy of the acceptor band. The question arises if it is possible to transfer the energy in photosynthetic complexes uphill ("uphill ET", $\varepsilon < 0$), when the energy of the donor band is positioned below the energy of the acceptor band (see Fig. 7). The answer is positive, and there exists significant experimental and theoretical research in this field. (See, for example, [55, 56, 57, 58, 59, 60, 61, 62], and references therein.) Even though many mechanisms of uphill ET are discussed in the literature, a complete understanding has not yet been reached.
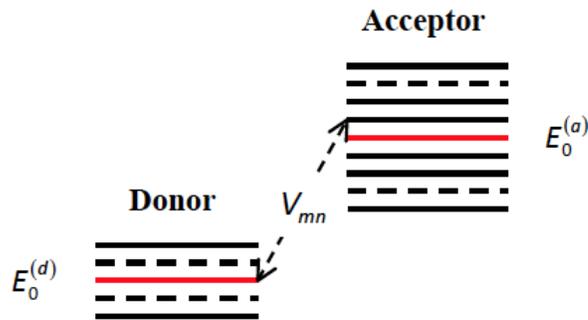
Figure 7. (Color online) Schematic of the uphill ET model consisting of the donor energy band positioned below the acceptor energy band.

In this sub-section, we discuss the uphill ET mechanism based on the 'entropy factor". Namely, we demonstrate that the uphill ET can be realized when the number of energy levels in the higher positioned acceptor band is larger than the number of energy levels in the lower positioned donor band, and under some additional conditions, which can be easily satisfied.

As was already mentioned, it was shown analytically and demonstrated numerically in [1] that for the asymptotic stationary solution in the discrete system of equations, described by the Hamiltonian (1), there is "equal distribution" of probabilities of all participating levels. Namely, for non-degenerate energy levels of the acceptor band $(\epsilon_{nn'} = E_n^{(a)} - E_{n'}^{(a)} \neq 0)$ at large time $(t \to \infty)$, the probability of population of any energy level, l, of donor and acceptor, is,

$$\langle \rho_{ll}(t \to \infty) \rangle = \frac{1}{2N_a + 2}, \tag{41}$$
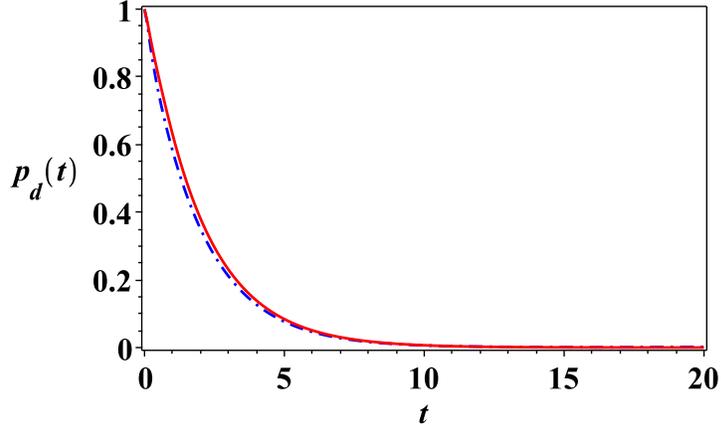
Figure 8. (Color online) Illustration of the uphill ET ($\varepsilon < 0$), shown in Fig. 9. Dependence of $p_d(t)$ on time. Discrete band (blue dash-dotted curve), continuous band (red solid curve). Parameters: $V = 0.25$ ($v = 2.528$), $\varepsilon = -20$, $D\sigma = 30$, $\gamma = 30$, $N_a = 50$, $\delta_a = 10$.
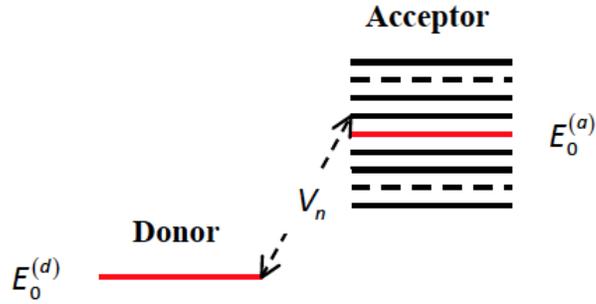
Figure 9. (Color online) Schematic of uphill ET model consisting of the donor with a single electron energy level positioned below the acceptor energy band.

where, as above, $2N_a + 1$ is the total number of levels in the acceptor band. This result is independent of whether we consider downhill ET or uphill ET.

We also observe independence of the ET on the sign of ε in our continuum approach. Namely, the above introduced dynamical rates, $\mathfrak{R}_1(t)$ and $\mathfrak{R}_2(t)$, do not depend on the sign of ε. So, the results will be the same for the acceptor band located above or below the donor energy level, with $E_0^{(d)} - E_0^{(a)} = \pm|\varepsilon|$. This means that our results for the ET dynamics, in the continuum approach, will be the same for both the downhill and uphill ET dynamics.

Then, the asymptotic probability to populate an acceptor band is:

$$p_a(t \to \infty) = \frac{2N_a + 1}{2N_a + 2}, \tag{42}$$

and $p_a(t \to \infty) \approx 1$, when $N_a \gg 1$. In the continuum limit, $N_a \to \infty$, and $p_d(t \to \infty) = 0$.

In Fig. 8, we present the results of numerical simulations for the uphill ET ($\varepsilon < 0$),

for the case shown in Fig. 9: a single-level donor and the acceptor with many quasi-degenerate levels, $2N_a + 1$. As one case see, the results for a discrete model (blue dash-dotted curve) are in good agreement with the results of our continuum approach (red solid curve).

A significant difference between the ET dynamics of the discrete and continuous models occurs when both the donor and the acceptor have finite bandwidths. This case is discussed in the next section.

3. Finite electron bands of donor and acceptor
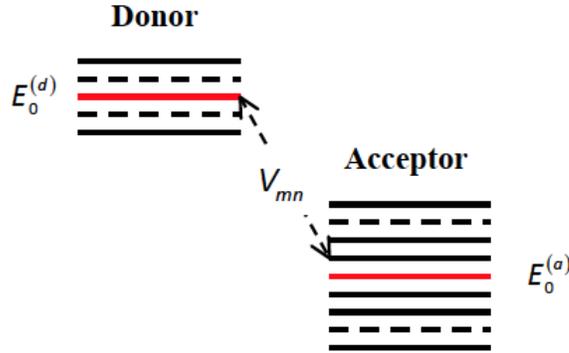
Figure 10. (Color online) Schematic of our model consisting of a donor and an acceptor with nearly continuous electron energy spectra.

In this Section, we consider both the donor and the acceptor sites with $2N_d + 1$ and $2N_a + 1$ nearly degenerate discrete energy levels, respectively (see Fig. 10). The corresponding Hamiltonian can be written as:

$$\mathcal{H}(t) = \sum_{m=-N_d}^{N_d} (E_m + \lambda_d(t))|m\rangle\langle m| + \sum_{n=-N_a}^{N_a} (E_n + \lambda_a(t))|n\rangle\langle n|$$
$$+ \sum_{m=-N_d}^{N_d} \sum_{n=-N_a}^{N_a} (V_{mn}|m\rangle\langle n| + V_{nm}|n\rangle\langle m|). \tag{43}$$

We assume that the electron energy spectra of both the donor and the acceptor are sufficiently dense, so in Eq. (43) one can perform an integration instead of the summation. We have,

$$\mathcal{H}(t) = \int (E_d + \lambda_d(t))|E_d\rangle\langle E_d|\varrho(E_d)dE_d + \int (E_a + \lambda_a(t))|E\rangle\langle E_a|\varrho(E_a)dE_a$$
$$+ \int\int dE_d dE_a \varrho(E_d)\varrho(E_a)\Big(V(E_d, E_a)|E_d\rangle\langle E_a| + \text{h.c.}\Big), \tag{44}$$

where, $\varrho(E_d)$, $\varrho(E_a)$, are densities of electron states in the donor and acceptor bands, respectively, and $V_{mn} \to V(E_d, E_a)$. Further, we assume that the amplitude of transition

is a smoothly varying function of energy, so one can approximate $V(E_d, E_a) \approx V$ as a constant.

For simplicity, we consider Gaussian densities of states for the donor and acceptor bands centered at $E_0^{(a)}$ for the acceptor and at $E_0^{(d)}$ for the donor,

$$\varrho(E_d) = \varrho_d e^{-\alpha_1 (E_d - E_0^{(d)})^2}, \tag{45}$$

$$\varrho(E_a) = \varrho_a e^{-\alpha_2 (E_a - E_0^{(a)})^2}. \tag{46}$$

The corresponding bandwidths of the donor and the acceptor can be defined as in Sec. II. Namely, the bandwidth of the donor is: $\delta_d = 2\sqrt{\pi/\alpha_1}$, and the bandwidth of the acceptor is: $\delta_a = 2\sqrt{\pi/\alpha_2}$.

The dynamics of the donor-acceptor complex can be described by the following rate-type system of ordinary differential equations (For detail see SM at http:// ...). We obtain,

$$\frac{d}{dt}\langle \rho_{11} \rangle = -\mathfrak{R}_1(t)\langle \rho_{11} \rangle + \mathfrak{R}_2(t)\langle \rho_{22} \rangle, \tag{47}$$

$$\frac{d}{dt}\langle \rho_{22} \rangle = \mathfrak{R}_1(t)\langle \rho_{11} \rangle - \mathfrak{R}_2(t)\langle \rho_{22} \rangle, \tag{48}$$

where

$$\mathfrak{R}_1(t) = \frac{\sqrt{\pi}\, v^2}{p} \left\{ \exp\left(-\frac{t^2}{2\alpha_1} + \frac{(t/2\alpha_1 - i\varepsilon)^2}{p^2} \right) \left(\mathrm{erf}\left(\frac{pt}{2} - \frac{(t/2\alpha_1 - i\varepsilon)}{p} \right) \right. \right.$$
$$\left. \left. + \mathrm{erf}\left(\frac{(t/2\alpha_1 - i\varepsilon)}{p} \right) \right) + \mathrm{c.c.} \right\}, \tag{49}$$

$$\mathfrak{R}_2(t) = \frac{\sqrt{\pi}\, v^2}{p} \left\{ \exp\left(-\frac{t^2}{2\alpha_2} + \frac{(t/2\alpha_2 - i\varepsilon)^2}{p^2} \right) \left(\mathrm{erf}\left(\frac{pt}{2} - \frac{(t/2\alpha_2 - i\varepsilon)}{p} \right) \right. \right.$$
$$\left. \left. + \mathrm{erf}\left(\frac{(t/2\alpha_2 - i\varepsilon)}{p} \right) \right) + \mathrm{c.c.} \right\}. \tag{50}$$

Here we have set, $\varepsilon = E_0^{(d)} - E_0^{(a)}$, and

$$v^2 = \frac{\pi \varrho_a \varrho_d |V|^2}{\sqrt{\alpha_1 \alpha_2}} = \frac{1}{4} \varrho_a \varrho_d \delta_a \delta_d |V|^2, \tag{51}$$

$$p = \sqrt{1/\alpha_1 + 1/\alpha_2 + 2(D\sigma)^2} = \sqrt{\delta_d^2/4\pi + \delta_a^2/4\pi + 2(D\sigma)^2}. \tag{52}$$

Note, that the parameters, v and p, generalize those defined in the previous sections in the case $N_d = 1$. The difference with the previous sections is that in (51), for finite $\delta_{a,d}$, we require that $v^2 \approx (2N_d + 1)(2N_a + 1)|V|^2 = \mathrm{const}$, when both $N_{a,d} \to \infty$ and $V \to 0$. As in the previous sections, this is equivalent to the requirement of a finite dispersion for the initial population of the donor band.

We find that the leading terms in Eqs. (49) and (50), as $t \to \infty$, are:

$$\mathfrak{R}_{1,2}(t) \sim \Gamma \cos\left(\frac{\varepsilon t}{\alpha_{1,2} p^2} \right) \exp\left(-\nu_{1,2} t^2 \right), \tag{53}$$

where

$$\Gamma = \frac{2\sqrt{\pi}v^2}{p}e^{-\varepsilon^2/p^2}, \tag{54}$$

$$\nu_{1,2} = \frac{2p^2 - 1/\alpha_{1,2}}{4\alpha_{1,2}p^2}. \tag{55}$$

Using the relationship between the bandwidths and the parameters $\alpha_{1,2}$, $\alpha_1 = 4\pi/\delta_d^2$, $\alpha_2 = 4\pi/\delta_a^2$, one can rewrite Eqs. (53), (55) as,

$$\mathfrak{R}_1(t) \sim \Gamma \cos\left(\frac{\delta_d^2 \varepsilon t}{4\pi p^2}\right) \exp\left(-\nu_1 t^2\right), \tag{56}$$

$$\mathfrak{R}_2(t) \sim \Gamma \cos\left(\frac{\delta_a^2 \varepsilon t}{4\pi p^2}\right) \exp\left(-\nu_2 t^2\right), \tag{57}$$

where,

$$\nu_1 = \frac{\delta_d^2(8\pi p^2 - \delta_d^2)}{64\pi^2 p^2}, \quad \nu_2 = \frac{\delta_a^2(8\pi p^2 - \delta_a^2)}{64\pi^2 p^2}. \tag{58}$$

Conditions of applicability of the rate-type equations. The conditions of validity of the approximation, leading to Eqs. (47) and (48), can be written as (see SM for technical details),

$$\left|D\sqrt{\chi(0)}\right| \ll \frac{d}{dt}\ln\chi(t)\Big|_{t=0} \ll \frac{3p^2}{2\varepsilon}, \tag{59}$$

$$\frac{v}{p} \ll 1, \quad \text{and} \quad \frac{|\Delta\rho(t)|}{p_a(t)} \ll 1. \tag{60}$$

They are similar to the conditions given by Eqs. (19) and (25). However, here the parameters, v and p, are given by (51) and (52), and the perturbation, $\Delta\rho(t)$, is defined by Eq. (121) in SM.

Inserting $p_a(t) = 1 - p_d(t)$ into Eq. (47), we obtain,

$$\frac{d}{dt}p_d = -(\mathfrak{R}_1(t) + \mathfrak{R}_2(t))p_d + \mathfrak{R}_2(t). \tag{61}$$

The solution is:

$$p_d(t) = e^{-f(t)}\left(p_d(0) + \int_0^t \mathfrak{R}_2(\tau)e^{f(\tau)}d\tau\right), \tag{62}$$

where $f(t) = \int_0^t (\mathfrak{R}_1(\tau) + \mathfrak{R}_2(\tau))d\tau$.

From here it follows, that if, for example, initially the donor was populated, $p_d(0) = 1$ (assume that the donor band is populated homogeneously), then, as $t \to \infty$, the asymptotic population of donor becomes,

$$\lim_{t\to\infty} p_d(t) = e^{-f(\infty)}\left(1 + \int_0^\infty \mathfrak{R}_2(\tau)e^{f(\tau)}d\tau\right). \tag{63}$$

Peculiarities of the ET dynamics for finite donor and acceptor bandwidths. When both the donor and acceptor bandwidths, δ_d and δ_a, are finite, the

ET dynamics is significantly different from the previous case of a simplified continuum model, with a single-level donor. This is mainly caused by the fact that both dynamical rates, $\mathfrak{R}_{1,2}(t)$, in (56) and (57) vanish, for the two-band model, at characteristic times, $t_{1,2} \sim 1/\sqrt{\nu_{1,2}}$, respectively. This was not the case for the simplified model, considered in Secs. II and III. [See Eqs. (32), (33), and (34)]. Namely, the parameter, Γ_1 in (32) has the meaning of the asymptotic rate. However, a similar (by its form) parameter, Γ, in (33) is a dynamical rate, which decays in time. This makes the ET dynamics of the simplified model and of the model with both finite donor and acceptor bands significantly different.

The rigorous mathematical approach for the transition from two discrete donor-acceptor energy bands to a continuum limit (including the intermediate dynamics), when $N_{d,a} \gg 1$ and $\delta_{d,a}$ are finite, will be discussed in the future. So far, we understand well the situation where the dimer is in contact with a quantum heat reservoir (not classical noise as in the present manuscript) in the limiting case when both bands are reduced to a single level, having arbitrary degeneracies N_d and N_a. In this situation we can apply the dynamical resonance theory [42] and find the population dynamics for all times explicitly, in both the Förster and the Marcus regime. Taking this as a starting point, we plan to develop the resonance theory also for finite (small) donor and acceptor bandwidths. We expect to observe the emergence of two time scales, similar to [63]. On a shorter time scale, the dynamics shows rich behavior due to the fact that there are multiple quasi-stationary states (corresponding to fully stationary states when the bandwidths collapse to zero). On a longer time scale the effect of the non-vanishing bandwidths becomes dominant and the dimer is driven to a final, unique stationary state (equilibrium).

Finally, the "intermediate" ET dynamics, in the continuum two-band model, significantly depends on three parameters, given by Eqs. (54) and (55): Γ, and $\nu_{1,2}$. Indeed, according to Eqs. (56) and (57), when $\Gamma \gg \sqrt{\nu_{1,2}}$, the ET dynamics reveals itself on the time-scale, $\sim 1/\Gamma$. And the relaxation effects, related to time-scales, $\sim 1/\sqrt{\nu_{1,2}}$, are not important. In this case, at some additional conditions (see below), one can expect a high efficiency of the ET from donor band to acceptor band. However, when $\Gamma \ll \sqrt{\nu_{1,2}}$, the ET dynamics is significantly suppressed, as the dynamical rates (56) and (57) quickly decay. In this case, for the initially populated donor band, one cannot expect an efficient ET to the acceptor band. Below, we plot the ET dynamics for initial population of the donor band, and for different values of the parameters.

When $\delta_d \ll \delta_a$, for times $t \gg 1/\delta_a$, one can neglect the contribution of the term $\int_0^t \mathfrak{R}_2(\tau) e^{f(\tau)} d\tau$, and (62) can be simplified as follows:

$$p_d(t) \approx e^{-\int_0^t \mathfrak{R}_1(\tau) d\tau}. \tag{64}$$

For an arbitrary donor bandwidth, we did not succeed to obtain an analytical expression for $p_d(t)$. However, for $\delta_d \ll \delta_a$ and $D\sigma \gtrsim \varepsilon/2$, we find that as $t \to \infty$, the

donor population can be estimated as,

$$p_d \approx \exp\left(-\frac{(2\pi)^{3/2}v^2}{p\delta_d}e^{-\varepsilon^2/p^2}\right). \tag{65}$$

This can be recast as follows:

$$p_d = \exp\left(-\frac{\sqrt{2}\pi\Gamma}{\delta_d}\right), \tag{66}$$

where Γ is defined by Eq. (54).

Let us assume that both bandwidths are of the same order: $\delta_a \approx \delta_d$. Supposing that $p_d(0) = 1$, we obtain from Eq. (62) the following result:

$$p_d(t) = \frac{1}{2}(1 + e^{-2\int_0^t \Re_1(\tau)d\tau}). \tag{67}$$

For $\delta_a, \delta_d \ll \varepsilon$ ($\delta_a \approx \delta_d$) and $D\sigma \gtrsim \varepsilon/2$, we find that asymptotically, as $t \to \infty$, the donor population is given by,

$$p_d(\infty) \approx \frac{1}{2}\left(1 + e^{-2\sqrt{2}\pi\Gamma/\delta_d}\right). \tag{68}$$

In Figs. 11 and 12, the results predicted by Eqs. (65), (68) and the numerical solution of Eq. (61) are presented. Our numerical simulations show that the asymptotic formulas (65) and (68) yield a good agreement with the solution of Eq. (61), when $D\sigma \gtrsim \varepsilon/2$.
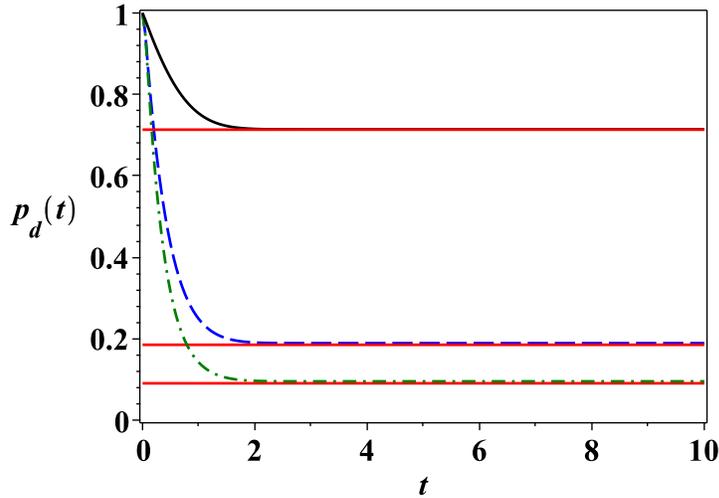
Figure 11. (Color online) Dependence of p_d on time ($v = 5$, $\delta_d = 5$, $\delta_a = 100$). Parameters: $D\sigma = 5$, $\varepsilon = 20$, $\gamma = 10$ (blue dashed curve) and $\varepsilon = 10$ (green dash-dotted curve); $D\sigma = 100$, $\varepsilon = 100$, $\gamma = 75$ (upper black solid curve). The results of the theoretical predictions, given by Eq. (65), are depicted by red lines.

Modified Wigner-Weisskopf, Förster, and Marcus-type ET dynamics. The parameters chosen in Fig. 11 are: $v = 5$, $\delta_d = 5$, $\delta_a = 100$, $D\sigma = 5$, $\gamma = 10$, $\varepsilon = 20$ (blue dashed curve) and $\varepsilon = 10$ (green dash-dotted curve). The lower green dash-dotted
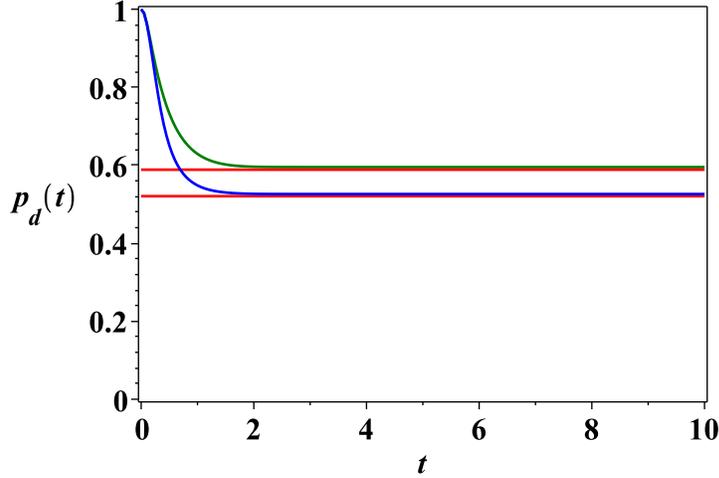
Figure 12. (Color online) Dependence of p_d on time ($v = 2$, $\varepsilon = 2$, $\delta_d = 5$, $\delta_a = 5$, $\gamma = 10$). From the top to bottom: $D\sigma = 10$ (green), $D\sigma = 5$ (blue). The results of the theoretical predictions, given by Eq. (68), are depicted by horizontal red solid lines

curve, represents the ET dynamics for the narrow donor band overlapped with the wide acceptor band, accompanied by a relatively weak dimer-noise interaction. We can say that this ET dynamics is of the Wigner-Weisskopf-type or of the Förster-type. For $\varepsilon = 100$ and $D\sigma = 100$ (black curve), the donor and acceptor bands do not overlap and we have the Marcus-type ET dynamics.

For the green dash-dotted curve, we chose $\Gamma \approx 1.7$, $\nu_1 \approx 1$, and $\nu_2 \approx 211$. So, we have: $\nu_1 < \Gamma \ll \nu_2$. In this case, the dynamical rate, $\mathfrak{R}_2(t)$, decays very fast (due to the relatively wide acceptor band), on the time-scale, $\sim 1/\sqrt{\nu_2} \approx 0.07$. The rate, Γ, provides the ET from donor band to acceptor band on the time-scale, $1/\Gamma \sim 0.6$. Finally, the dynamical rate $\mathfrak{R}_1(t)$, decays on the time-scale, $\sim 1/\sqrt{\nu_1} \approx 1$, and the ET dynamics saturates. In this case, the efficiency of the ET from donor to acceptor is, $p_a(t \to \infty)\rangle \approx 90\%$. (See Fig. 11, green dash-dotted curve.)

On the other hand, for parameters: $v = 5$, $\varepsilon = 100$, $\delta_d = 5$, $\delta_a = 100$, $D\sigma = 100$ the donor and acceptor bands do not overlap, and the dimer-noise interaction is strong (close to the resonant noise, $p = \sqrt{2}\varepsilon$). So, we can say that the upper black curve in Fig. 11 corresponds to the Marcus-type ET dynamics.

In this case, $\Gamma \approx 0.337$, $\nu_1 \approx 1$, and $\nu_2 \approx 400$. So, we have: $\nu_1 \lesssim \Gamma \ll \nu_2$. Similar to the previous case, the dynamical rate, $\mathfrak{R}_2(t)$, decays very fast, on the time-scale $\sim 1/\sqrt{\nu_2} \approx 0.05$. Because $\nu_1 \lesssim \Gamma$, the ET dynamics saturates, as in the previous case, at the time-scale, $\sim 1/\sqrt{\nu_1} \approx 1$. Because Γ is smaller than in the previous case, the ET efficiency drops to $\approx 30\%$. (See Fig. 11, black curve.)

In Fig. 12, the Marcus-type ET rate is plotted, $\Gamma \approx (\sqrt{2\pi}v^2/2D\sigma)\exp(-\varepsilon^2/2D^2\sigma^2)$. In this case, the dimer-noise interaction constant is relatively large, $D\sigma \gg \delta_{d,a}/\sqrt{8\pi}$, for all values of $D\sigma$, presented in Fig. 12. Because the donor and acceptor bandwidths

are equal, the efficiency is not high. For example, for $D\sigma = 10$, the rate $\Gamma \approx 0.86$, and $\nu_{1,2} \approx 0.25$. The efficiency in this case is approximately 40%. When the dimernoise interaction decreases, $D\sigma = 5$, we have: $\Gamma \approx 1.59$, and $\nu_{1,2} \approx 0.25$. In this case, the efficiency increases, and reaches approximately 48%.   In Figs. 13 – 15, the
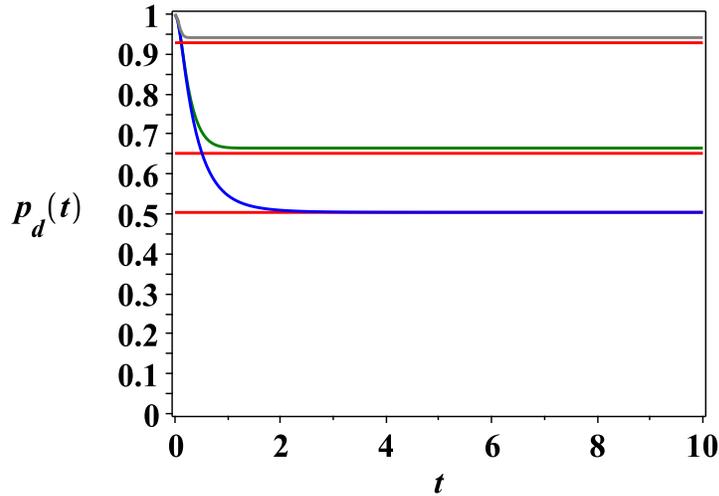
Figure 13. (Color online) Dependence of p_d on time, ($\varepsilon = 5$, $v = 2.5$, $D\sigma = 10$, $\gamma = 15$). From the top to bottom: $(\delta_d, \delta_a) = [(50, 50), (10, 10), (2.5, 2.5)]$. The results of the theoretical predictions, given by Eq. (68), are depicted by the horizontal red solid lines.
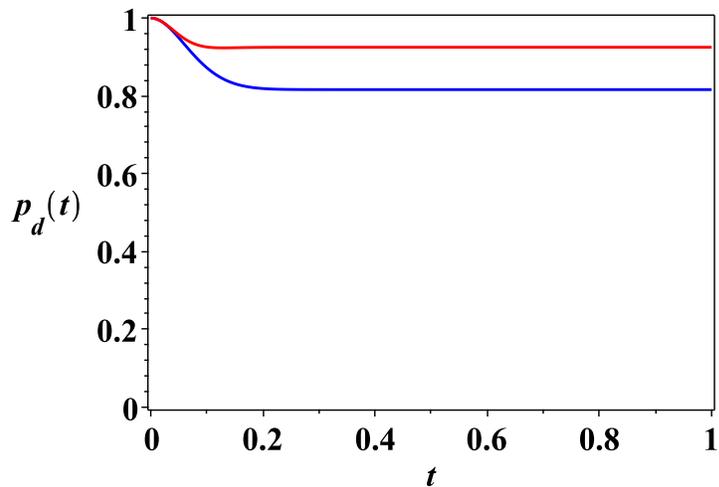
Figure 14. (Color online) Dependence of p_d on time, ($\varepsilon = 0$, $v = 5$, $D\sigma = 1$, $\gamma = 10$). From the top to bottom: $(\delta_d, \delta_a) = [(100, 50), (50, 100)]$.

dependence of the donor population, $p_d(t)$, is shown for different values of parameters. For parameters chosen in Fig. 13, both bands have equal widths. For a relatively weak
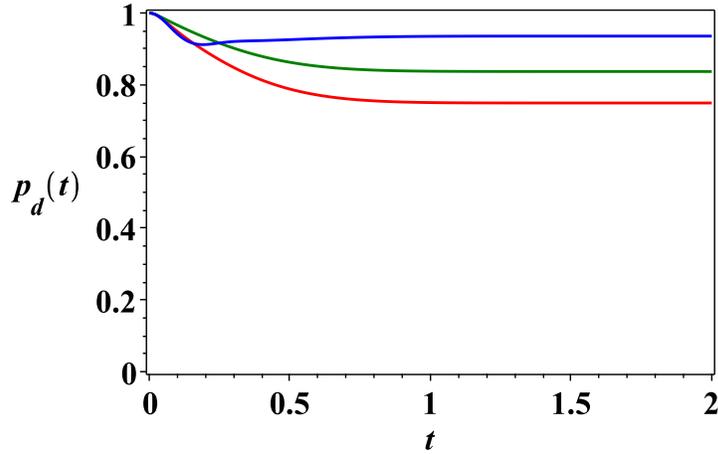
Figure 15. (Color online) Dependence of p_d on time, ($\varepsilon = 20$, $v = 3$, $\delta_d = 10$, $\delta_a = 25$, $\gamma = 75$). From the top to bottom: $D\sigma = 5, 50, 20$.
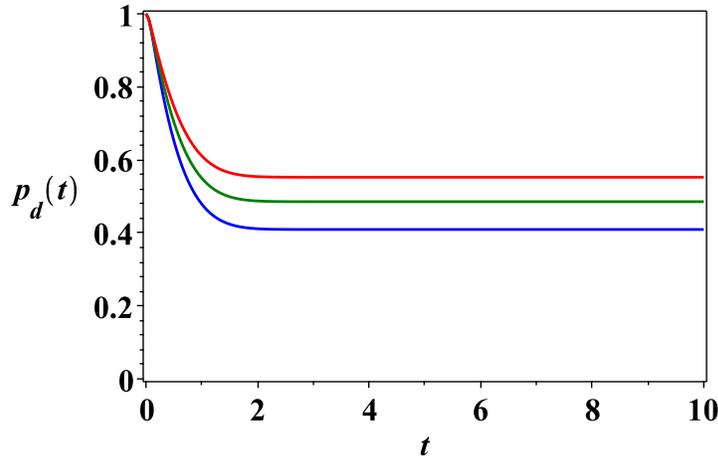
Figure 16. (Color online) Uphill ET for two finite bands. Dependence of p_d on time, ($\varepsilon = -5$, $v = 2.5$, $\delta_d = 5$, $\delta_a = 10$, $\gamma = 15$). From the top to bottom: $D\sigma = 20, 15, 10$.

dimer-noise interaction, the efficiency of population of the acceptor band is small (upper red curve). When the dimer-noise interaction is strong, and both bands are narrow (blue lower curve in Fig. 13), the results become close to those of the two-level system. In this case, the populations of donor and acceptor bands become close.

When the donor band is wider than the acceptor band (red curve in Fig. 14), the acceptor is not efficiently populated. In this case, $\Gamma \approx 3$, $\nu_1 \approx 239$, and $\nu_2 \approx 90$. Then, in this case, both dynamical rates, $\mathfrak{R}_{1,2}$ decay fast, and the efficiency of acceptor population is small.

Finally, as the bandwidth of the acceptor increases, the population of the acceptor becomes more efficient (blue lower curve in Fig. 14). Similar results, with different intensity of noise, are presented in Fig. 15. More efficient population of the acceptor,

for $D\sigma = 20$, occurs because this case is closer to the resonant one, $p = \sqrt{2}\varepsilon$.

Uphill ET dynamics. Since the dynamical rates, $\mathfrak{R}_1(t)$ and $\mathfrak{R}_2(t)$, 53, do not depend on the sign of ε, the results for the ET dynamics are the same for the acceptor band located above or below the donor band (see Figs. 7 and 10). In Fig. 16, we present the results of numerical simulations for the uphill ET ($\varepsilon < 0$), for different values of the dimer-noise interaction constant, $D\sigma$. For chosen parameters, indicated by the green curve, the efficiency of the uphill acceptor population reaches 60%.

4. Conclusion

In this paper, we have studied the exciton and electron transfer (ET) dynamics using a donor-acceptor model in which both the donor and the acceptor are represented by continuous energy bands of finite width. Direct interactions between the donor and the acceptor are described by matrix elements in the Hamiltonian. Instead of the thermal bath, we model the environment by a stationary stochastic process which acts on both the donor and the acceptor energy levels.

The usefulness of our approach is that it allowed us (i) to derive a set of simplified rate-type differential equations, which describe the ET dynamics, and (ii) to present *analytically* the generalized expressions for the time dependent "dynamical ET rates". They are characterized by the redox potential (distance between bands), a single parameter - a sum of the contributions from the dimer-noise interaction constant and the bandwidths of donor and acceptor, and some time-independent decay rates. These generalized ET rates allowed us to derive analytically the ET rates for Wigner-Weisskopf, Förster-type, and Marcus-type limits.

We presented numerical simulations which illustrate and confirm our analytical results. We demonstrated that by manipulating the bandwidths of donor and acceptor, high efficiency of acceptor population can be achieved for both downhill and uphill, sharp and flat redox potentials. We have paid particular attention to the formulation of the conditions of applicability of the simplified rate-type equations for the ET dynamics.

Experimental tests of our results would be useful for a simplified description of complex bio-systems. One possibility is to separate the contributions to the exciton (electron) transfer coming from (i) the thermal bath and noise, associated with the protein-solvent environment and (ii) the entropy factor – the contribution to the ET rates related to the finite widths of electron donor and acceptor bands. Indeed, as we have demonstrated, the dimer-noise interaction constant and the bandwidths enter the asymptotic expression for the ET rate through a dimensionless parameter called p. Experiments measuring the ET rate and the efficiency (in which the bandwidths of both donor and acceptor and their overlap can be controlled) can be performed, for example, by using the photosynthetic bio-complexes based on chlorophyll molecules. Another possibility is to use the artificial nano-systems considered in [4, 5]. In this case, both donor and acceptor are two dye molecules embedded in a DNA-engineered environment [64]. In these experiments, the Wigner-Weisskopf, Förster-type, and Marcus-type limits

can be studied for downhill and uphill, sharp and flat redox potentials.

Acknowledgments

Appendix A. Comparison of continuum and discrete models

In this section, we compare the discrete system governed by the Hamiltonian (1) with the corresponding continuous model, described by the rate-type Eqs. (15) and (16). We assume, for simplicity, that the amplitudes of transitions, V_n, are the same for all acceptor levels, $V_n = V$. We consider the noisy environment to be described by a random
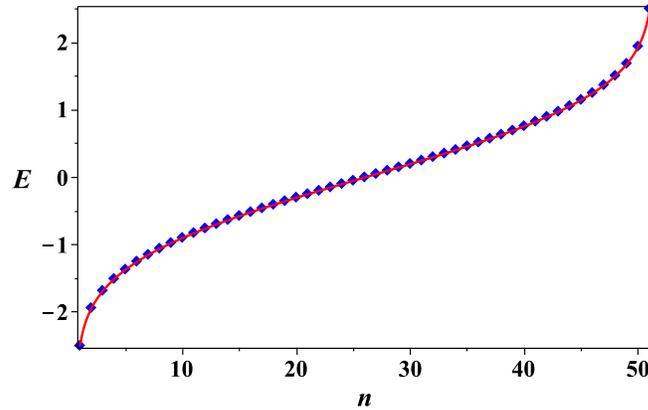
Figure A1. (Color online) Energy distribution inside the acceptor band: discrete band (blue diamonds), continuous band (red solid curve). Parameters: $N_a = 25$, $\delta_a = 5$.

telegraph process with the correlation function given by,

$$\chi(t - t') = \sigma^2 e^{-2\gamma|t-t'|}, \tag{A.1}$$

where σ is the amplitude of noise, and γ is the decay rate of correlations. It is convenient to introduce the subindex 0 to denote the donor level, while $n = 1, \ldots, 2N_a + 1$ denotes the nth acceptor level (this notation is different from the one previously used in the paper). Then, the equations of motion can be written as follows (for details see Ref. [1]):

$$\langle \dot{\rho}_{00} \rangle = iV \sum_{n=1}^{M} (\langle \rho_{0n} \rangle - \langle \rho_{n0} \rangle), \tag{A.2}$$

$$\langle \dot{\rho}_{nn'} \rangle = -i\epsilon_{nn'}\langle \rho_{nn'} \rangle + iV(\langle \rho_{n0} \rangle - \langle \rho_{0n'} \rangle),$$

$$\langle \dot{\rho}_{0n} \rangle = i\epsilon_{n0}\langle \rho_{0n} \rangle + iV(\langle \rho_{00} \rangle - \sum_{n'=1}^{M}\langle \rho_{n'n} \rangle) - iD\sigma\langle \rho_{0n}^{\xi} \rangle,$$

$$\langle \dot{\rho}_{00}^{\xi} \rangle = -2\gamma\langle \rho_{00}^{\xi} \rangle + iV\sum_{n=1}^{M}(\langle \rho_{0n}^{\xi} \rangle - \langle \rho_{n0}^{\xi} \rangle),$$

$$\langle \dot{\rho}_{nn'}^{\xi} \rangle = (i\epsilon_{n'n} - 2\gamma)\langle \rho_{nn'}^{\xi} \rangle + iV(\langle \rho_{n0}^{\xi} \rangle - \langle \rho_{0n'}^{\xi} \rangle),$$

$$\langle \dot{\rho}_{0n}^{\xi} \rangle = (i\epsilon_{n0} - 2\gamma)\langle \rho_{0n}^{\xi} \rangle + iV(\langle \rho_{00}^{\xi} \rangle - \sum_{n'=1}^{M}\langle \rho_{n'n}^{\xi} \rangle) - iD\sigma\langle \rho_{0n} \rangle, \qquad (A.3)$$

where $\epsilon_{n'n} = E_{n'}^{(a)} - E_n^{(a)}$, $\epsilon_{n0} = E_n^{(a)} - E_0^{(d)}$ and $\langle \rho_{nn'}^{\xi} \rangle = \langle \xi(t)\rho_{n,n'}(t) \rangle$.

Further, we assume that $M = 2N_a + 1$ acceptor levels are distributed inside the band, centered at the point $E_0^{(a)} = E_{N_a+1}^{(a)}$, and according to the Gaussian distribution (3). We find the following relation between the label n of the energy levels and their energies,

$$n = N_a + 1 + \frac{N_a\mathrm{erf}\left(\dfrac{2\sqrt{\pi}(E_n^{(a)} - E_{N_a+1}^{(a)})}{\delta_a}\right)}{\mathrm{erf}(\sqrt{\pi})}. \qquad (A.4)$$

Solving this relation for $E \equiv E_n^{(a)}$ yields the curve plotted in Fig. A1.

Employing Eq. (5), one can recast the renormalized amplitude of transition, $v^2 = V^2\varrho_0\sqrt{\pi/\alpha}$, as

$$v = V\sqrt{\frac{2N_a + 1}{\mathrm{erf}(\sqrt{\pi})}}. \qquad (A.5)$$

According to the definitions in (12), and Eqs. (19) and (25), the conditions of validity of the continuum approximation, (19), are given by,

$$\frac{|\Delta\rho(t)|}{p_a(t)} \ll 1, \quad \text{and} \quad \frac{v}{p} \ll 1, \qquad (A.6)$$

$$|D\sigma| \ll 2\gamma \ll \frac{3p^2}{3\varepsilon}, \qquad (A.7)$$

where $\Delta\rho(t)$, is defined below Eq. (51) in SM.

It is important to note, that in the region of parameters (A.7), the ET rate (28) does not depend on the decay rate, γ, of the noise correlation function (A.1). In our numerical simulations, presented in Figs. A3 – 8 for selected parameters, the second condition in Eq. (A.6) and the inequalities, (A.7), are satisfied for all cases, except for those presented in Figs. A5 and A9. The first condition in Eq. (A.6) is analyzed in the Appendix in SM.

In Fig. A2, we plot the population distribution, $\langle \rho_{ii}(t) \rangle$, inside the discrete acceptor band, for different times. As one can see, the evolution of $\langle \rho_{ii}(t) \rangle$ approaches, for large times, an "equal distribution" [1] (black diagonal crosses in Fig. A2, for $t = 1000$). The energy level of the donor and of each acceptor is populated with equal probability, $1/(2N_a + 2)$. With $N_a = 25$, this gives $\langle \rho_{ii}(t \to \infty) \rangle = 1/(2N_a + 2) \approx 0.019$.
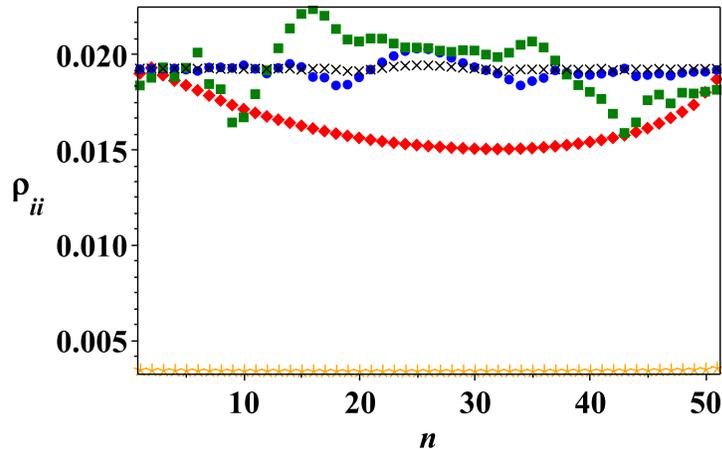
Figure A2. (Color online) Population distribution inside the discrete acceptor band, for different times, t: $t = 1$ (orange asterisks), $t = 10$ (red diamonds), $t = 100$ (green boxes), $t = 500$ (blue circles), $t = 1000$ (black diagonal crosses). Parameters: $V = 0.25$, $\varepsilon = 20$, $D\sigma = 40$, $\gamma = 30$, $\delta_a = 5$, $N_a = 25$.

In Figs. A3 - A5, we compare the results of numerical simulations for discrete and continuous acceptor bands, for the Marcus-type ET rate, for different parameters, and for $N_a = 50$. So, the total number of levels in the acceptor band is, $2N_a + 1 = 101$. When both conditions of validity of continuous approximation, (A.6) and (A.7), hold, one can observe a good agreement between the discrete and continuum models (Figs. A3 and A4).

In Fig. A5, we compare the regime of the Marcus-type ET for discrete and continuous models, and for the choice of parameters when the first inequality in (A.6) is violated, and the rate-type Eqs. (15) and (16) cannot be used. (For details see Appendix C in SM at http://....)

Intermediate ET dynamics for weak and strong dimer-noise interaction and narrow acceptor band

For a continuous acceptor band, and for any (even a very small) asymptotic rate, Γ_1 (28), the probability of population of a single-level donor approaches zero as $t \to \infty$: $p_d(t \to \infty) = 0$. However, our simulations show that there can be a two-scale ET dynamics of the donor-acceptor system. Indeed, suppose that the acceptor band is relatively narrow. Then, on an *intermediate* time scale, the dynamics resembles the dynamics of a two-level system (with $\delta_a \approx 0$, see (A.8)) and after, on a longer time scale given by $t_{slow} \sim 1/\Gamma_1$, a slow re-population of the acceptor band occurs.

In Fig. A6, we show the intermediate dynamics of the initially populated donor for a weak dimer-noise interaction constant ($D\sigma = 0.01$) and for a relatively narrow acceptor band, $\delta_a < \varepsilon$ ($\delta_a = 2$, $\varepsilon = 10$). In this case, the intermediate dynamics approaches the dynamics of the corresponding two-level "donor-acceptor" system, in which noise
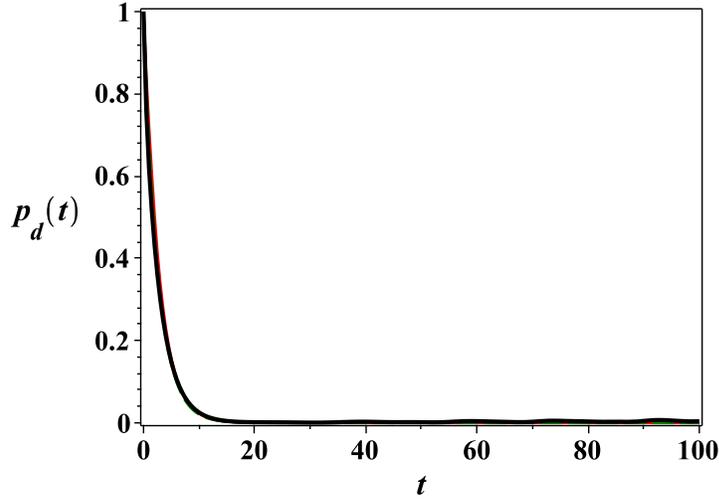
Figure A3. (Color online) The Marcus-type ET. Dependence of the donor probability, $p_d(t)$, on time. Discrete band (blue curve), continuum band (red curve). Green dashed curve corresponds to an exponential decay with the rate given by Eq. (39). Parameters: $V = 0.25$, $(v = 2.528)$, $\varepsilon = 10$, $D\sigma = 40$, $\gamma = 60$, $\delta_a = 5$, $N_a = 50$.
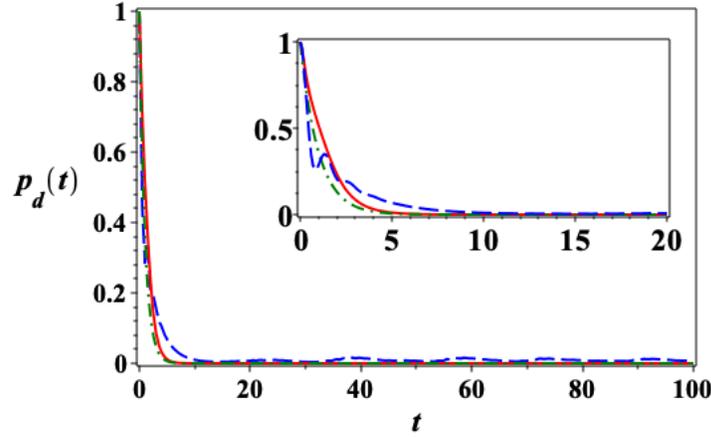
Figure A4. (Color online) The Marcus-type ET. Dependence of the donor probability, $p_d(t)$, on time. Discrete band (blue dashed curve), continuum band (red solid curve). Green dash-dotted curve corresponds to an exponential decay with the rate given by Eq. (39). The inset is a zoom of the main figure, to show the initial system behavior. Parameters: $V = 0.2$, $(v = 2.02)$, $\varepsilon = 1$, $D\sigma = 10$, $\gamma = 30$, $\delta_a = 5$, $N_a = 50$.

is absent. In the latter case, we found empirically that the solution of Eqs. (A.2) and (A.3) for $p_d(t)$ can be approximated as,

$$p_d(t) = 1 - \frac{4v^2}{\varepsilon^2 + 4v^2}\left(1 - e^{-\nu t^2}\cos(\Omega_R t)\right), \tag{A.8}$$

where $\nu = \delta_a^2/16\pi$ [see (34)] and $\Omega_R = \sqrt{\varepsilon^2 + 4v^2}$. The amplitude of oscillations of $p_d(t)$ is found to be, $4v^2/(\varepsilon^2 + 4v^2)$. As one can see from (A.8), the Rabi oscillations
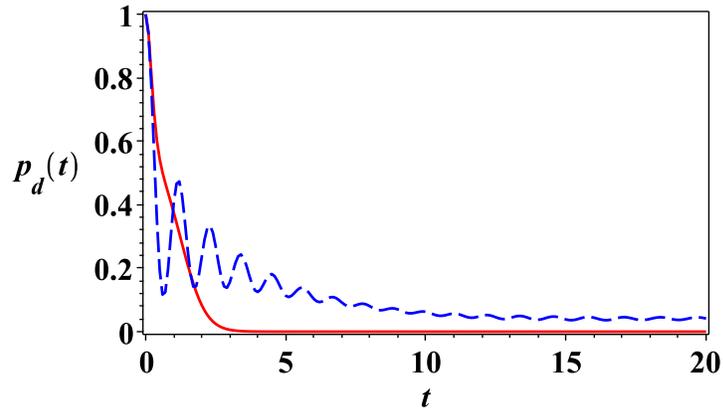
Figure A5. (Color online) Dependence of the donor probability, $p_d(t)$, on time, when the condition (A.6) of applicability of the continuum approach is violated. Discrete band (blue dashed curve), continuous band (red solid curve). Parameters: $V = 0.249$, $(v = 2.5)$, $\varepsilon = 0$, $D\sigma = 5$, $\gamma = 15$, $\delta_a = 5$, $N_a = 50$.
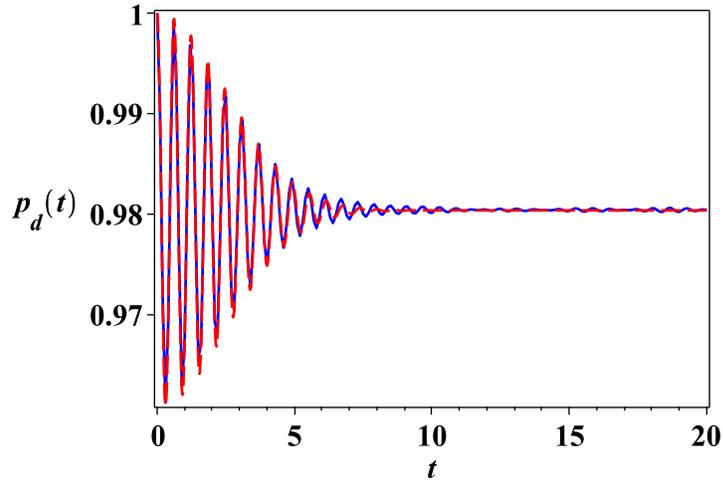
Figure A6. (Color online) The two-level system limit: narrow acceptor band and weak noise. Dependence of $p_d(t)$ on time. Parameters: $N_a = 50$, $\varepsilon = 10$, $\delta_a = 2$, $D\sigma = 0.005$, $\gamma = 0.01$, $V = 0.1$. Blue curve presents the solution of the discrete model, described by the system of Eqs. (A.2) and (A.3). Red dashed curve corresponds to the analytical expression (A.8).

decay. For the parameters chosen in Fig. A6, $p_d^{min} \approx 0.98$, and the period of oscillations, $T = 2\pi/\Omega_R \approx 0.616$. Figure A6 shows a good agreement of analytical expression (A.8) with the numerical solution for the discrete band. The decay of the Rabi oscillations resulted from the finite width of the acceptor band.

In Figs. A7 and A8, we compare the results of the numerical simulations for discrete and continuum acceptor bands, for a narrow acceptor band and for a weak dimer-noise interaction, and when the conditions of applicability of the continuum approximation,
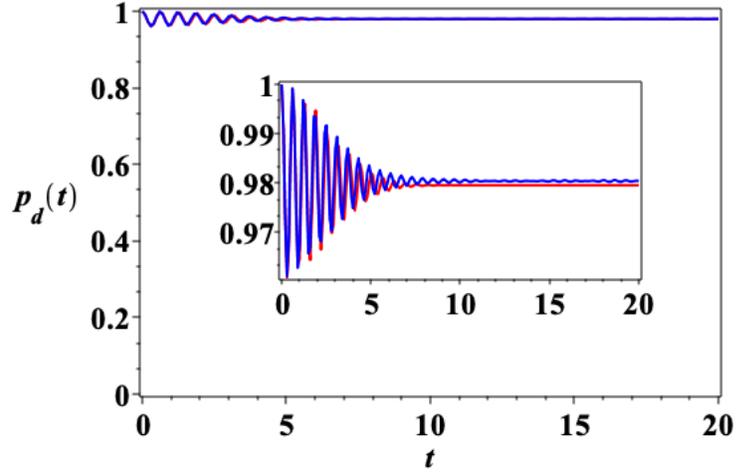
Figure A7. (Color online) The two-level system limit: narrow acceptor band and weak dimer-noise interaction. Dependence of $p_d(t)$ on time. Parameters: $N_a = 50$, $\varepsilon = 10$, $\delta_a = 2$, $D\sigma = 0.005$, $\gamma = 0.01$, $V = 0.1$ $(v = 1.01)$. Red curve corresponds to the results of rate-type Eqs. (15) and (16), which describe the ET in the continuous acceptor band mode. The blue curve presents the solution of the discrete model described by Eqs. (A.2) and (A.3). The inset shows the zoom-in of the main figure.
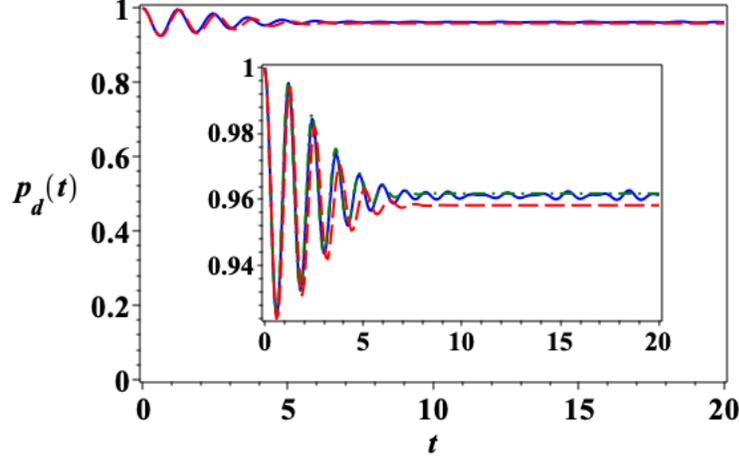
Figure A8. (Color online) The two-level system limit: narrow acceptor band and weak dimer-noise interaction. Dependence of $p_d(t)$ on time, t. Parameters: $N_a = 25$, $\varepsilon = 5$, $\delta_a = 2$, $D\sigma = 0.01$, $\gamma = 0.025$, $V = 0.1$ $(v = 0.719)$. The blue curve presents the solution of the discrete model described by Eqs. (A.2) and (A.3). The red dashed curve corresponds to the analytical expression (A.8). The green dash-dotted curve corresponds to the results of Eqs. (15) and (16) (continuous acceptor band). The inset shows the zoom-in of the main figure.

(A.6) and (A.7), are satisfied. One can observe a good agreement between discrete and continuum models.

As was mentioned above, for very large times, the probability of the donor
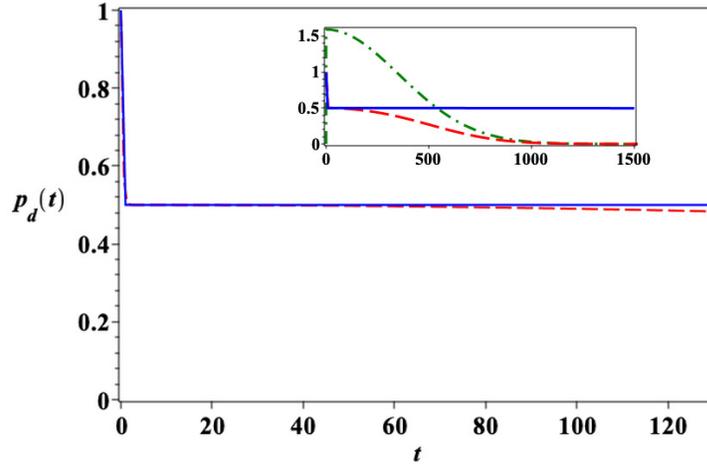
Figure A9. (Color online) The two time-scale behavior of the system for strong dimer-noise interaction and narrow band. Parameters: $N_a = 50$, $\varepsilon = 5$, $\delta_a = 0.01$, $D\sigma = 40$, $\gamma = 60$, $V = 0.5$ ($v = 5.06$). Red dashed curve corresponds to the solution of Eqs. (15) and (16) (continuous band). Blue curve represents the solution of the discrete model described by the system of Eqs. (A.2) and (A.3). The inset shows the asymptotic behavior of the continuum model (red dashed curve), of the discrete system (blue solid curve, $N_a = 25$) and of the dynamical rate $\mathfrak{R}_2(t)$ (green dash-dotted curve).
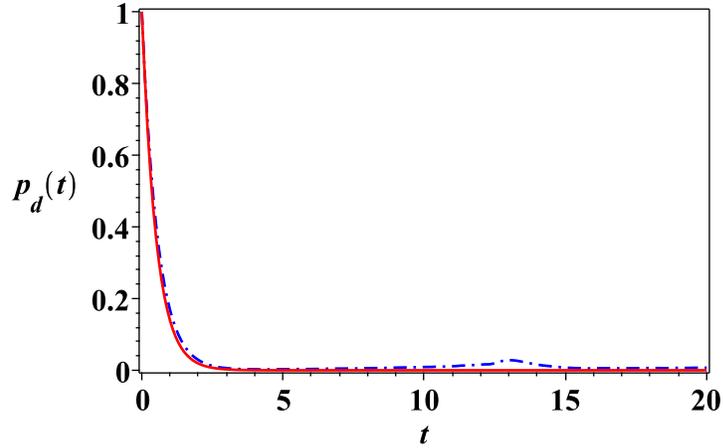
Figure A10. (Color online) The Marcus-type ET, for strong dimer-noise interaction and narrow band. Dependence of $p_d(t)$ on time. Parameters: $N_a = 50$, $\varepsilon = 150$, $\delta_a = 100$, $D\sigma = 150$, $\gamma = 100$, $V = 1.39$ ($v = 14$). Blue dash-dotted line presents the solution of the discrete model described by the system of Eqs. (A.2) and (A.3). Red curve corresponds to the results of Eqs. (15) and (16) (continuous band).

population, $p_d(t \to \infty) = 0$, and the acceptor becomes populated. For parameters chosen in Figs. A6, A7 and A8, the characteristic timescale, at which the ET dynamics approaches its intermediate asymptotics [take $t \to \infty$ in A.8]

$$p_d \approx \frac{\varepsilon^2}{\varepsilon^2 + 4v^2}, \tag{A.9}$$

can be estimated as: $t_{sat} = 1/\sqrt{\nu} \approx 2/p \approx 4\sqrt{\pi}/\delta_a \approx 3.5$. The intermediate asymptotics (A.9) and the saturation time, t_{sat}, are in good agreement with numerical results for both the discrete and continuum models.

In Fig. A9, we show the intermediate ET dynamics close to the two-level system, for narrow acceptor band and for strong dimer-noise interaction. The pure two-level system, with $\delta_a = 0$, and all other parameters as in Fig. A5, experiences, for large enough times, the equal distribution, $p_d(t) = p_a(t) = 1/2$ [1]. As one can see from Fig. A9, at intermediate time already, $t \approx 100$, the equal distribution is approximately realized in a continuum model. Because of finite width of the acceptor band, δ_a, the probability, $p_d(t)$, decays in both, discrete and continuous systems. However, an important observation is that both curves start to diverge significantly after $t \approx 100$, due to inapplicability of the rate-type equations. Similar to Figs. A6 - A8, the intermediate ET dynamics occurs, after which a slow exponential decay of the donor population takes place with a very small ET rate (see inset in Fig. A9).

Example: Dimers based on *Chla* ***and*** *Chlb* ***molecules in LHCs.*** The energy transfer from *Chlb* (donor) to *Chla* (acceptor) occurs on the $0.1 - 10$ ps timescale [65], depending on the geometry of the LHC, the matrix elements of interaction between donor and acceptor, and the environment, as well as the positioning of the dimer in the local protein-solvent environment. As a representative example, we mention here ref. [66], where the exciton Hamiltonian pertaining to the first excited states of chlorophyll (*Chla* and *Chlb*) pigments in the minor light-harvesting complex CP29 of plant photosystem II is determined based on the recent crystal structure at 2.8 Å resolution applying a combined quantum chemical/electrostatic approach as used earlier for the major light-harvesting complex LHCII.

In Fig. A10, we compare the discrete and continuum models for a strong dimer-noise interaction and for a relatively narrow band (Marcus-type ET). The chosen parameters are: $\varepsilon = 150\,\text{ps}^{-1} \approx 100\,\text{meV}$, $v = 14\,\text{ps}^{-1} \approx 9.3\,\text{meV}$, $\delta_a = 100\,\text{ps}^{-1} \approx 66.7\,\text{meV}$, $D\sigma = 150\,\text{ps}^{-1} \approx 100\,\text{meV}$, which are close to the parameters of the donor-acceptor dimers realized by *Chla* and *Chlb* molecules in LHCs. (See, for example, [66], and references therein.) For the given choice of parameters, the conditions of validity of approximation (A.6) and (A.7) hold, and one can see a good agreement between the two models. The analytical expressions for the ET rate (28) (or (39)) give, $\Gamma_1 \approx 2\,\text{ps}^{-1}$, which is in good agreement with numerical simulations.

References

[1] S. Gurvitz, A.N. Nesterov, and G.P. Berman, J. Phys. A: Math. Theor., **50**, 365601 (2017).

[2] S. Gurvitz, Front. Phys., **12**, 120303 (2017).

[3] X. Li, Front. Phys., **11**, 110307 (2016).

[4] S. Buckhout-White, M. Ancona, E. Oh, J.R. Deschamps, M.H. Stewart, J.B. Blanco-Canosa, P.E. Dawson, E.R. Goldman, and I.L. Medintz, ACS Nano, **6**, 1026 (2012).

[5] C.M. Spillmann, M.G. Ancona, S. Buckhout-White, W.R. Algar, M.H. Stewart, K. Susumu, A.L. Huston, E.R. Goldman, and I.L. Medintz, ACS Nano, **7(8)**, 7101 (2013).

[6] M. Mohseni, Y. Omar, G. Engel, and M.B. Plenio (eds.), Quantum Effects in Biology (Cambridge University Press, 2014).

[7] K.L.M. Lewis, F.D. Fuller, J.A. Myers, C.F. Yocum, S. Mukamel, D. Abramavicius, and J. P. Ogilvie, J. Phys. Chem. A, **117**, 34 (2012).

[8] G. Engel, T. Calhoun, E. Read, T. Ahn, T. Mancal, Y. Cheng, R. Blankenship, and G. Fleming, Nature Letters **446**, 782 (2007).

[9] A. Ishizaki and G.R. Fleming, J. Chem. Phys., **130**, 234110 (2009).

[10] A. Ishizaki and G. Fleming, PNAS **106**, 17255 (2009).

[11] E. Collini, C. Wong, K. Wilk, P. Curmi, P. Brumer, G. Scholes, Nature Letters **463**, 644 (2010).

[12] G. Panitchayangkoon, D. Hayes, K. Fransted, J. Caram, E. Harel, J. Wenb, R. Blankenship, G. Engel, PNAS USA **107**, 12766 (2010).

[13] D.M. Wilkins and N.S. Dattani, J. Chem. Theory Comput. **11**, 3411 (2015).

[14] P. Rebentrost, M. Mohseni, I. Kassal, S. Lloyd, and A. Aspuru-Guzik, New J. Phys. **11**(3), 033003 (2009).

[15] G. Celardo, F. Borgonovi, M. Merkli, V. Tsifrinovich, and G. Berman, J. Phys. Chem. **116**, 22105 (2012).

[16] D.I.G. Bennett, K. Amarnath, and G.R. Fleming, JACS, **135**, 9164 (2013).

[17] R. Marcus and N. Sutin, Biochimica et Biophysica Acta, **811**, 265 (1985).

[18] X. Hu, A. Damjanovic, T. Ritz, and K. Schulten, Proc. Natl. Acad. Sci. USA **95**, 5935 (1998).

[19] M. Merkli, G.P. Berman, R.T. Sayre, S. Gnanakaran, M. Könenberg, A.I. Nesterov, and H. Song, J. Math. Chem., **54**, 866 (2016).

[20] S. Gurvitz, G.P. Berman, and R.T. Sayre, Europ. Phys. J. Special Topics, **227** 2349 (2019).

[21] S. Santabarbara, G. Agostini, A.P. Casazza, C.D. Syme, P. Heathcote, F. Böhles, M.C.W. Evans, R.C. Jennings, and D. Carbonera, Biochimica et Biophysica Acta, **1767** 88 (2007).

[22] J. Du, T. Teramoto, K. Nakata, E. Tokunaga, and T. Kobayashi, Biophysical Journal, **101**, 995 (2011).

[23] A. Pascal, E. Peterman, C. Gradinaru, H. van Amerongen, R. van Grondelle, and B. Robert, J. Phys. Chem. B, **104**, 9317 (2000).

[24] B. McMahon, P. Fenimore, and M. LaBute, in *Fluctuations and Noise in Biological, Biophysical, and Biomedical Systems*, *Proceedings of SPIE*, vol. 5110, ed. by S.M. Bezrukov, H. Frauenfelder, F. Moss (2003), *Proceedings of SPIE*, vol. 5110, pp. 10 – 21

[25] T.G. Dewey and J.G. Bann, Biophysical Journal, **63**, 594 (1992).

[26] R. Grima, J. Chem. Phys., **132**, 185102 (2010).

[27] P. Carlini, A.R. Bizzarri, and S. Cannistraro, Physica D, **165**, 242 (2002).

[28] M.S. Samoilov, G. Price, and A.P. Arkin, Science's STKE, **2006**, re17 (2006).

[29] G. Juzeliūnas and D.L. Andrews, Advs. in Chem. Phys., **112**, 357 (2000).

[30] A.G. Redfield, Adv. Magn. Reson, **1**, 1 (1965).

[31] M. Yang and G. Fleming, Chem. Phys., **282**, 161 (2002).

[32] Yu-H. Hwang-Fu, W. Chen, and Y.C. Cheng, Chemical Physics, **447**, 46 (2015).

[33] D.P.S. McCutcheon and A. Nazir, J. Chem. Phys., **135**, 114501 (2011).

[34] L. Yang, M. Devi, and S. Jang, J. Chem. Phys., **137**, 024101 (2012).

[35] J.M. Moix and J. Cao, J. Chem. Phys., **139**, 134106 (2013).

[36] X. Chen, J. Cao, and R.J. Silbey, J. Chem. Phys., **138**, 224104 (2013).

[37] C.Y. Hsieh and J. Cao, J. Chem. Phys., **148**, 014103 (2018).

[38] C.Y. Hsieh and J. Cao, J. Chem. Phys., **148**, 014104 (2018).

[39] A. Govorov, P.L.H. Martínez, and H.V. Demir (Eds.), Understanding and Modeling Förster-type Resonance Energy Transfer (FRET), Introduction to FRET, Vol. 1 (Springer, 2016).

[40] V.F. Weisskopf and E.P. Wigner, Z. Physics **63**, 54 (1930).

[41] S. Mukamel, *Principles of Nonlinear Optical Spectroscopy* (Oxford University Press, 1995).

[42] M. Merkli, I.M. Sigal, and G.P. Berman, Phys. Rev. Lett. **98**, 130401 (2007).

[43] M. Merkli, G.P. Berman, and A. Redondo, J. Phys. A, Math. Theor., **44**, 305306 (2011).

[44] J. Bergli, Y.M. Galperin, and B.L. Altshuler, New Journal of Physics, **11**, 025002 (2009).

[45] Y.M. Galperin, B.L. Altshuler, J. Bergli, D. Shantsev, and V. Vinokur, Phys. Rev. B **76**, 064531 (2007).

[46] A.I. Nesterov and G.P. Berman, Phys. Rev. A, **85**, 052125 (2012).

[47] P.W. Milonni and S.M.H. Rafsanjani, Phys. Rev. A, **92**, 062711 (2015).

[48] V.E. Shapiro and V.M. Loginov, Physica **90A**, 563 (1978).

[49] V. Klyatskin, *Dynamics of Stochastic Systems* (Elsevier, 2005).

[50] V. Klyatskin, *Lectures on Dynamics of Stochastic Systems* (Elsevier, 2011).

[51] A.I. Nesterov, G.P. Berman, J.M. Sánchez Mártinez, and R. Sayre, J. Math. Chem., **51**, 1 (2013).

[52] M. Abramowitz, I.A. Stegun (eds.), *Handbook of Mathematical Functions* (Dover, 1965).

[53] W.S. Struve, In: Anoxygenic Photosynthetic Bacteria, R.E. Blankenship, M.T. Madigan and C.E. Bauer (Eds.), Chapter 15, p. 297 (Kluwer Academic Publishers, 1995).

[54] T. Förster, Ann. Phys. (Leipzig) **2**, 55 (1948).

[55] V.V. Shubin, I.N. Bezsmertnaya, and N.V. Karapetyanpanel, J. Photochemistry and Photobiology B: Biology, **30**, 153 (1995).

[56] M. Mimuro, K. Hirayama, K. Uezono, H. Miyashita, and S. Miyachi, Physica Acta, **1456**, 27 (2000).

[57] H. Sumi, J. Phys. Chem. B, **106**, 13370 (2002).

[58] H. Sumi, J. Phys. Chem. B, **108**, 11792 (2004).

[59] P. Loughlin, Y. Lin, and M. Chen, Photosynth Res., **116**, 277 (2013).

[60] S. I. Allakhverdiev, V. D. Kreslavski, S. K. Zharmukhamedov, R. A. Voloshin, D. V. Korolyakova, T. Tomo, and J.R. Shen, Biochemistry (Moscow), **81**, 201-212 (2016).

[61] M. Kaucikas, D. Nürnberg, G. Dorlhiac, A.W. Rutherford, and Jasper J. van Thor, Biophysical Journal, **112**, 234 (2017).

[62] L.M. Tan, J. Yu, T. Kawakami, M. Kobayashi, P. Wang, Z.Y.W. Otomo, and J.P. Zhang, J Phys. Chem. Lett., **9**, 3278 (2018).

[63] M. Merkli, H. Song, an G.P. Berman, J. Phys. A: Math. Theor. **48**, 275304 (2015).

[64] N.C. Seeman, J. Theor. Biol., **99**, 237 (1982).

[65] T.K. Ahn, T.J. Avenson, M. Ballottari, Y.C. Cheng, K.K. Niyogi, R. Bassi, and G.R. Fleming, Science, **320**, 794 (2008).

[66] F. Müh, D. Lindorfer, M. Schmidt am Busch, and T. Renger, Phys. Chem. Chem. Phys., **16**, 11848 (2014).